Charles University in Prague
Faculty of Mathematics and Physics

DIPLOMA THESIS

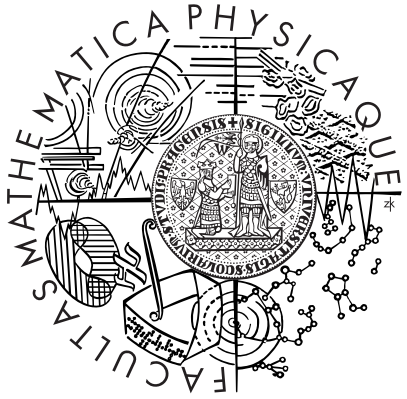

Jiří Procházka

Elastic proton collisions at high energies

Institute of Particle and Nuclear Physics

Supervisor: RNDr. Vojtěch Kundrát, DrSc.
Institute of Physics of the ASCR, v.v.i.

Field of study: Physics, Nuclear and Particle Physics

Prague 2009

First of all I would like to thank to my supervisor Dr. Vojtěch Kundrát for perfect collaboration and tireless help during working on this thesis. I would like to thank also to Dr. Mario Deile and Mgr. Jan Kašpar, who were my supervisors during my stay at CERN in summer 2008, for their dedication and patience. I also appreciate great help and support of other people from the TOTEM collaboration. Many meetings and discussions, which I had with them helped me to obtain experience and insight not only into TOTEM's physics programme.

Last but not least I would like to express my deep gratitude to my family for permanent support and extraordinary helpful atmosphere.

I declare that I completed my diploma thesis myself and with use of cited literature only. I agree with using this thesis.

Prague, 9th April 2009 (corrected version)

Jiří Procházka

Contents

List of Figures

List of Tables

Title: Elastic proton collisions at high energies
Author: Jiří Procházka
Department: Institute of Particle and Nuclear Physics
Supervisor: RNDr. Vojtěch Kundrát, DrSc.
Institute of Physics of the ASCR, v.v.i.
Supervisor's e-mail address: kundrat@fzu.cz

Abstract: The thesis consists of two parts. The first part is devoted to the study of pp-induced background at $\beta^* = 0.5$ m optics in the TOTEM Roman Pot system. The response of TOTEM Roman Pot (RP) silicon detectors will be simulated for particles taken from an existing simulation of this kind of background. In the second part, we shall analyze pp (resp. $\bar{p}p$) experimental data obtained earlier at energy of 52.8 GeV (resp. 541 GeV) with the use of two phenomenological models of elastic hadronic amplitude which have been used already earlier in similar analyses by other authors. The first model is based on assumption of constant hadronic phase (i.e., constant quantity $\rho(s,t)$) in the whole region of kinematically allowed values of t; and the second one, proposed by Brazil group, represents one of the present models with hadronic phase that exhibits a certain t-dependence. Some consequences of the models concerning the profile functions in the impact parameter space, which have not bean earlier studied, will be shown. To perform all necessary fits and to systematize different models and approaches describing elastic pp or $\bar{p}p$ scattering new program written in C++ has been developed.

Keywords: elastic proton scattering, TOTEM experiment, Roman Pot background

Název práce: Pružné srážky protonů při vysokých energiích
Autor: Jiří Procházka
Katedra (ústav): Ústav částicové a jaderné fyziky
Vedoucí bakalářské práce: RNDr. Vojtěch Kundrát, DrSc.
Fyzikální ústav AVČR, v.v.i.
e-mail vedoucího: kundrat@fzu.cz

Abstrakt: Předkládaná práce se skládá ze dvou částí. První část je věnována studiu pp-indukovaného pozadí v římských hrncích experimentu TOTEM při optice $\beta^* = 0.5$ m. Pro částice z existujicí simulace tohoto pozadí bude dále simulována odezva silikonových detektorů umístěných v římských hrncích. V druhé části budou analyzována pp (resp. $\bar{p}p$) experimentální data obdržená dříve při energii 52.8 GeV (resp. 541 GeV) s užitím dvou fenomenologických modelů elastické hadronové amplitudy, které již byli užity v podobných analýzách různými autory. První model je založen na předpokladu, že hadronová fáze je konstantní (tj. veličina $\rho(s,t)$ je konstantní) v celém rozsahu kinematicky přípustných hodnot t; a druhý model, navrhovaný brazilskou skupinou, představuje jeden ze současných modelů s t-závislou hadronovou fází. Některé dosud nestudované důsledky těchto modelů týkající se profilových funkcí budou ukázány. Aby bylo možné provést všechny potřebné fity a systematizovat různé modely a přístupy popisující elastický pp nebo $\bar{p}p$ rozptyl, nový program napsaný v C++ byl vyvinut.

Klíčová slova: elastický rozptyl protonů, experiment TOTEM, pozadí v římských hrncích

Chapter 1

Introduction

The first proton-proton (pp) interactions at higher energies were observed in the CERN Intersecting Storage Rings (ISR), the world's first hadron collider, in 1971. Many interesting experiments have been performed since that time. The purpose of all these experiments is to learn more about structure of fundamental particles. A number of remarkable properties were discovered.

In the following the attention will be devoted mainly to elastic proton-proton interactions. Two of four fundamental interactions (forces) play significant role in such a case - the electromagnetic and the strong interactions.

First of them, the electromagnetic, is also called the Coulomb interaction. Protons, as charged particles with electric charge $+e$, are repelled mutually by this interaction. The second interaction, the strong interaction, is attractive and is called hadronic or nuclear because this strong interaction sticks together different nucleons (i.e., protons and neutrons) in a nucleus. The strong interaction is short-ranged in contrast to the Coulomb interaction which is regarded as long-ranged. Hadronic force overcomes the electric repulsion between protons in the nucleus.

Elastic scattering is in principle the most simple scattering where the same incident particles come out after the collision. Characteristics of these processes such as cross section depend only weakly on energy. On the other hand the average number of produced particles in inelastic collisions and corresponding cross section depend strongly on energy. The elastic collisions represent always a significant part of processes at any energy. There is, however, a smaller part of inelastic processes that exhibit similar energy behavior. They are denoted as diffractive processes. One assumes that one particle or both the incident particles are brought in the collision to an excited state which decays then into several secondary particles, all moving in original direction. One speaks about single or double diffraction. The majority of the rest of collision events are denoted as non-diffractive inelastic. In contrast to diffractive ones, they are strong energy dependent and the final secondary particles have large transverse momenta.

In spite of the fact that since 1971 many experimental data have been gathered there is no reliable theory of pp (resp. $\bar{p}p$) diffractive processes. There are only several different models which more or less well describe present experimental data on phenomenological grounds.

To learn more about the structure of fundamental particles it is necessary to improve and extend present experimental data of diffractive processes. This is one of the main purpose why new Large Hadron Collider (LHC) is being built now at European Organization for Nuclear Research (CERN). It will provide high intensity proton collisions

with center of mass energy up to 14 TeV.

The six LHC experiments will study what will occur if the corresponding LHC beams collide. One of them is TOTEM (TOTal Elastic and diffractive cross section Measurement) experiment that will be devoted mainly to study of elastic processes. As discussed in Letter of Intent in 1997 [1], the TOTEM experimental programme was proposed to measure (see also [2] and [3])

- **the total proton-proton cross section** with an absolute error of 1 mb by using the luminosity independent method. It requires simultaneous measurement of pp elastic scattering at low momentum transfer and of the total inelastic rate.
- **elastic scattering** in the largest possible interval of four-momentum transfer $-t \approx p^2\vartheta^2$ from the Coulomb region $-t \approx 10^{-3}$ GeV^2 up to the nuclear region $-t \approx 10$ GeV^2
- the **diffractive dissociation**, including single and double diffraction

This thesis consists of two parts: study of background in the TOTEM RPs and theoretical description of elastic pp and $\bar{p}p$ scattering together with an analysis of experimental data obtained earlier with use of two phenomenological models of hadronic amplitude. The first part has been done during the stay of the author of this thesis at CERN in summer 2008 [4].

The TOTEM RP system is essential for detection of diffractive protons. However, detection of diffractive protons (signal) is always accompanied by other particles (background). To achieve the goals of the TOTEM experiment good knowledge of the proton background is, therefore, important for developing background suppression algorithm. In Chapter 2, we will firstly present briefly TOTEM RP system essential for detection of diffractive protons. Then we will use an existing simulation of a pp-induced background at $\beta^* = 0.5$ m optics to show which particles may enter RPs. The response of TOTEM RP silicon detectors for the most important background particles will be demonstrated with use of TOTEM RP simulation and reconstruction software. The study of the response of the RP silicon detectors is one of the first steps towards developing a background suppression algorithm which is in general very complicated task.

Chapter 3 is devoted to the theoretical description of pp (resp. $\bar{p}p$) elastic scattering which is essential for reaching the challenging TOTEM goals. We will present two formulas for complete elastic amplitude $F^{C+N}(s,t)$ which determines elastic differential cross section and takes into account both the Coulomb and hadronic interactions. The first one (historically older) is West and Yennie formula and the second is general formula derived on the basis of the eikonal model. We will also introduce the elastic hadron scattering amplitude in the impact parameter space.

In Chapter 4, we shall go back to pp (resp. $\bar{p}p$) experimental data obtained earlier at energy of 52.8 GeV (resp. 541 GeV). We will discuss two different models of elastic hadronic amplitude $F^N(s,t)$: the model with constant hadronic phase and that proposed by Brazil group. Some consequences of the models also in the impact parameter space will be shown. Similar analyses for different models of hadronic amplitude were done, e.g., in [5] or [6].

To perform all the necessary fits newly developed program written in C++ will be used. It is used in fitting a hadronic amplitude $F^N(s,t)$ to measured pp or $\bar{p}p$ elastic

differential cross section at given energy and computes some other physically significant quantities introduced in Chapter 3.

Chapter 2

Roman Pot background studies

Detection of diffractive protons (signal) is always accompanied by other particles (background). To achieve the goals of the TOTEM experiment good knowledge of the proton background is important. In this chapter we will briefly introduce TOTEM RP system essential for detection of diffractive protons. After that, we will take advantage of an existing simulation of pp-induced background to show which particles may be produced at the Interaction Point 5 (IP5) and which ones may enter RPs detectors. Finally, we will demonstrate the response of TOTEM RP silicon detectors for the most important background particles with use of TOTEM RP simulation and reconstruction software. The study of the response of the RP silicon detectors is one of the first steps towards developing an effective background suppression algorithm.

2.1 TOTEM Roman Pot system

Diffractive protons at hight energies are scattered to very small angles in the beam pipe. If the beam has not stable position and shape (before stabilization) then it is necessary to hold detectors far from the beam. After stabilization of the beam the detectors may be moved near to the beam. To detect particles in the beam pipe the detectors are placed in movable beam insertions - called Roman Pots (RPs) so that the detectors inside the RPs can be moved near or far from the beam. They are placed inside a secondary vacuum vessel (called a pot) and moved into the primary vacuum of the machine through vacuum bellows. The primary vacuum is then preserved against an uncontrolled out-gassing of the detector's materials by a thin window.

To detect protons as close to the beam as possible novel planar silicon detectors with so-called Current Terminating Structure (CTS) have been developed, see [7]. All TOTEM RP silicon detectors have the CTS on one edge which faces the beam. The CTS collects the current generated in the highly damaged region at the cut edge and so avoids its diffusion into the sensitive volume. The active volume starts already at ≈ 50 μm from the physical edge. This is the reason why this kind of detectors is called "edgeless". Each detector has 512 strips with pitch of 66 μm. The strips in the detectors are at angle of 45° with respect to the edge facing the beam.

Each TOTEM RP will be equipped with a stack of 10 edgeless silicon strip detectors. Half of them will have their strips oriented at angle of $+45°$ with respect to the edge facing the beam, and the other half at angle of $-45°$. The measurement of each track projection in five planes is advantageous for the reduction of uncorrelated background via programmable coincidences, requiring, e.g., collinear hits in a majority of the planes

and so selecting only particles at small angles with respect to the beam axis.

To reconstruct protons in very forward region from both sides of the IP5, TOTEM uses RP system which is symmetric with respect to IP5. TOTEM RP system consists of 4 RP stations, 2 stations on both sides of IP5 at distances of ±147 m and ±220 m, see Fig. 2.1. A RP station is an ensemble of 2 RP units, each unit consists of two vertical and one horizontal RPs. The TOTEM RP system has thus 24 RPs in total.

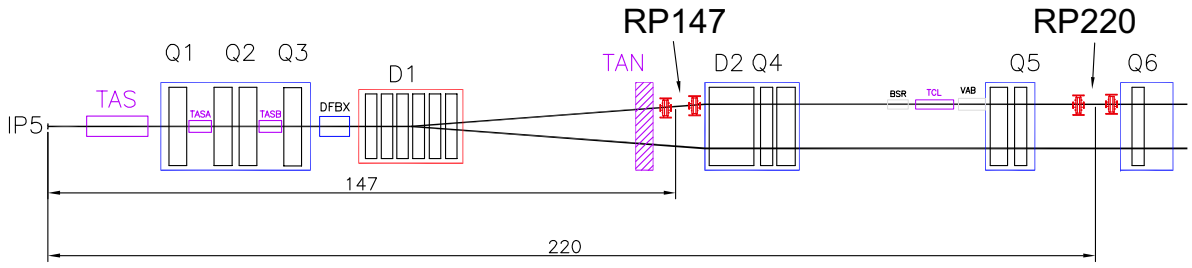

Figure 2.1: The LHC beam line on the "right" side of the Interaction Point 5 (IP5) and the TOTEM RP stations at distances of 147 m (RP147) and 220 m (RP220).

2.2 Background in the Roman Pots

The RP silicon detectors will not detect only diffractively scattered protons at IP5 interesting for the TOTEM experiment (signal) but they will also detect a lot of other particles (background). Good knowledge of the background at all RP stations plays, therefore, an important role in the development of the background suppression algorithms.

One may distinguish three kinds of machine-induced background in RPs (see [8]):

- The **beam halo** consisting of beam protons that were lost from their design orbits and were not caught by the collimation system.
- The **beam-gas** background caused by shower particles created by collisions between protons and gas molecules which are present in the beam pipe.
- The **beam-beam** (pp) background which is caused by generic inelastic proton-proton collisions in IP5 producing a great number of particles in the forward direction. The produced particles may propagate through the LHC ring to the RP stations and even further. On their way along the beam line they may also collide with machine elements and create secondary showers.

2.3 Simulation of background in the Roman Pots

To study the background in the RPs one may start with its simulation. One may generate same diffractive events (signal) and mix them with non-diffractive events (background) to simulate actual experiment.

This kind of simulation was made by V. Talanov in CERN. It is based on generic p-p interactions at energy of $\sqrt{s} = 14$ TeV in IP5. The particles created in IP5 are

transported to RP147 and RP220 at $\beta^* = 0.5$ m optics so that the interaction with all machine elements is included. β^* is the value of betatron function at IP5. Only the pp-induced background was taken into account. A simulation of the response of RP strip detectors is not included in this simulation (we will extend this simulation in the next sections).

The simulation is available at the CASTOR[1] in the directory /castor/cern.ch/user/t/talanov/Public/2007. Mainly following three files containing simulated events were used:

- **IP5**
  This file contains diffractive as well as non-diffractive events produced from the primary p-p collisions (10^6 events) at energy of $\sqrt{s} = 14$ TeV in IP5. The cut on pseudo-rapidity[2] $|\eta| > 7.8$ corresponding to the aperture of TAS absorber is included, see Fig. 2.1. The events were generated using the Monte Carlo event generator DPMJET. Only the "right" part of the p-p source, particle entering LSS5R (right side of Long Straight Section (LSS) of the interaction point IP5), was taken into account.

- **RP147**
  This file corresponds to the previous one. The particles produced at IP5 are then transported through the LHC ring to the RP147 station; interactions with all machine elements (see [7] and [9]) are included. This file contains particles recorded at a scoring plane at the start of the space reserved for TOTEM between the TAN absorber and the dipole magnet D2 at 148.63 m, see Fig. 2.1. Only particles within a radius of $r < 4$ cm around the beam position were recorded. This corresponds to the size of the LHC beam pipe. This sample of protons contains protons created in interaction with machine elements as well as protons transported directly without interaction from IP5.

- **RP220**
  This file was created in a similar manner as the previous one, just the scoring plane was at 214.252 m (in front of RP220).

Hundreds of plots were produced with the aim to understand the simulations. For this purpose a standalone program written in C++ using ROOT [10] libraries has been made. It reads *events* from the simulation and selects *particles* with chosen characteristics.

The distribution of particle types at IP5 is ploted in Fig. 2.2. We may see that pions, protons and neutrons are the most produced particles at IP5. The distribution of particle types entering RP147 and RP220 taking into account geometrical acceptance of three detectors is shown in Fig. 2.3. These distributions of particle types at RP147 and RP220 are more interesting for our background studies. Mainly photons (dominant component), electrons, positrons and pions entering RP147 and RP220 strip detectors. All characteristics (angular distribution, hit distribution, energy distribution,...) of electrons are very similar to positrons. Similarly, the characteristics of π^+ are practically the same as characteristics of π^-.

[1] CASTOR stands for CERN Advanced STORage manager

[2] The pseudo-rapidity η is defined by $\eta \equiv -\log(\tan(\vartheta/2))$, where ϑ is the forward angle

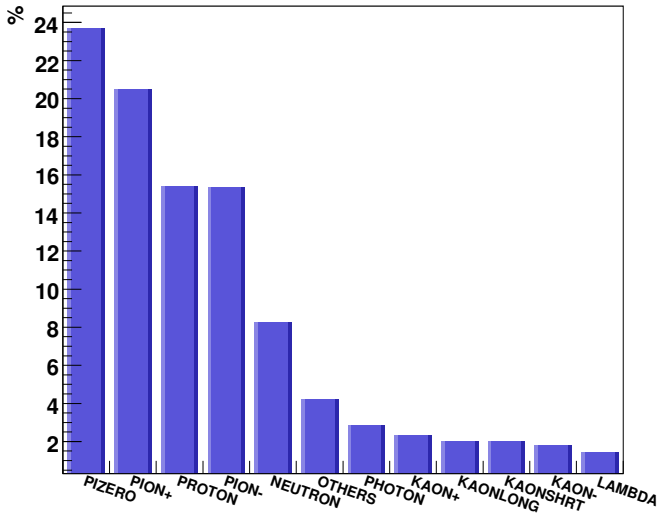

Figure 2.2: Distribution of particles at IP5 (3662661 particles).

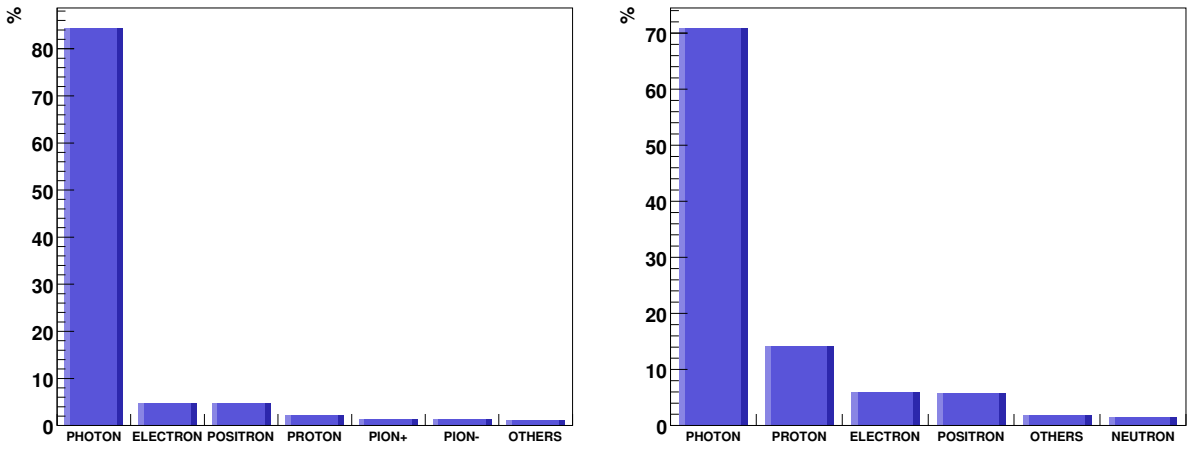

(a) RP147 (205702 particles)

(b) RP220 (33846 particles)

Figure 2.3: Distribution of particles at (a) RP147 and (b) RP220 taking into account the geometrical acceptance of two vertical and one horizontal RP detectors.

Proton hit distributions at RP147 and RP220 are shown in Fig. 2.4. Only the hits within the geometrical acceptance of the silicon detectors are displayed. Majority of protons (both at RP147 and RP220) would be detected in the horizontal detectors.

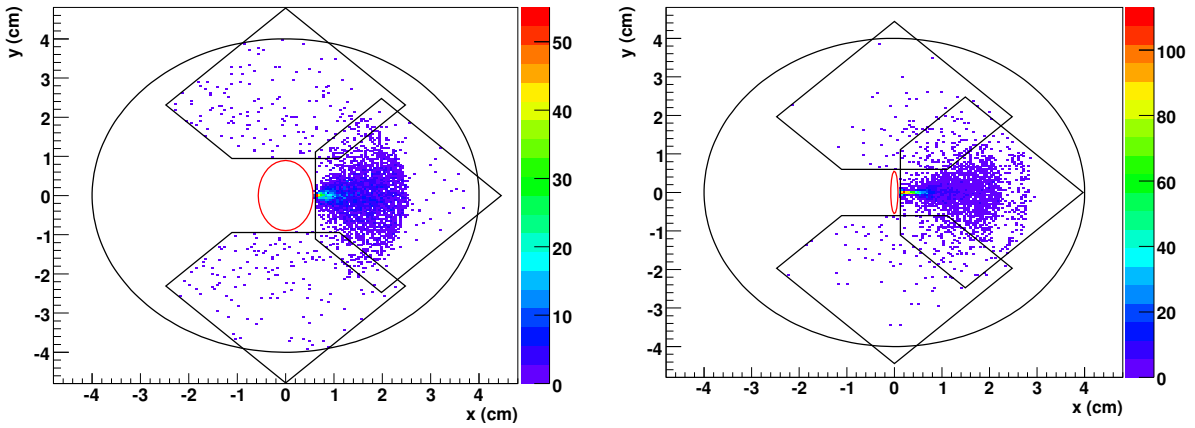

(a) RP147 (4508 particles)

(b) RP220 (4775 particles)

Figure 2.4: Hit distribution of protons at (a) RP147 and (b) RP220 taking into account the geometrical acceptance of two vertical and one horizontal detectors. The circle with radius 4 cm represent the beampipe (x and y axises have different scaling). Positive value of x corresponds to the direction from the center of the LHC ring. Positive value of y corresponds to up direction.

It is worth to mention that there are also *primary neutral* particles in the acceptance of the RP147 and RP220 directly from IP5. This is one of two open questions relating to the simulations. The second open question is the existence of two *separated* groups in the angular distribution of electrons, positrons and photons at RP147, see Fig. 2.5. The particles from the left group have higher energy than the particles from the right group.

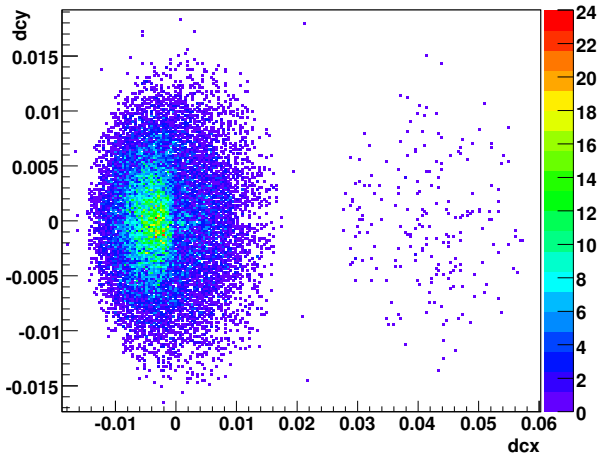

Figure 2.5: Angular distribution of electrons at RP147. Direction cosine is defined by $dcx = \frac{\vec{p}.\vec{x}}{p}$ where $\vec{p}$ is the momentum of a particle and the direction $\vec{x}$ corresponds to the direction from the center of the LHC ring. Similarly for direction cosine dcy, see also the legend of Fig. 2.4.

2.4 TOTEM RP simulation and reconstruction chain

To study the response of the RP silicon strip detectors for particles from the previous simulation we may create a "source" module containing these particles and plug it to the TOTEM simulation and reconstruction chain.

We may divide the simulation part in our case into two steps. The first step consists of simulation of deposition of the energy of a particle from the source module entering the RP strip detectors. This simulation is done by Geant4. The second step contains digitalization, i.e., conversion of the energy to the strip hits.

This simulation of strip hits can be afterward taken as an input to the TOTEM RP reconstruction chain which is schematically shown in Fig. 2.6, see [11].

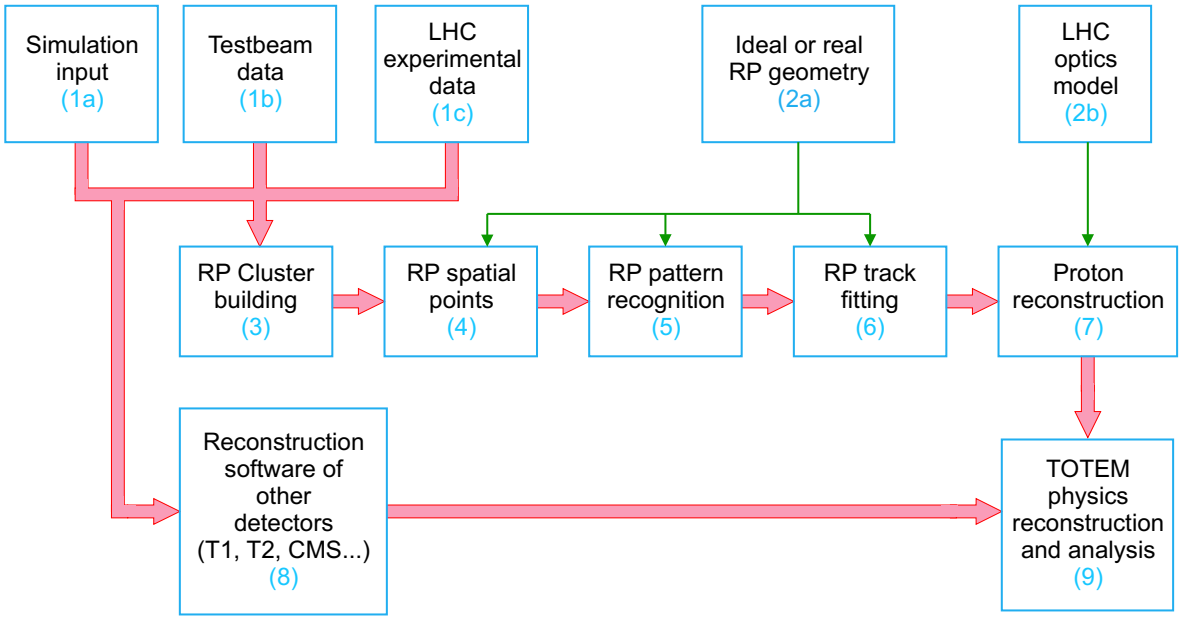

Figure 2.6: Work flow diagram of the TOTEM RP reconstruction software.

The TOTEM RP reconstruction chain is the same for simulated input (1a), testbeam data (1b) or real LHC experimental data (1c). The strip hits are transformed into strip cluster (3) and then converted, with the help of geometry information (2a), into spatial points (4). The pattern recognition module (5) is responsible for finding the proton track candidates from the spatial points. The road search algorithm is applied to find the candidates approximately parallel to the beam. The RP track candidates are fitted by the straight line (6). Finally, the aim of the proton reconstruction modules (7) is determination of the proton tracks in the RP (local reconstruction) or finding the proton kinematics at IP5 (global reconstruction). This reconstruction is different for different LHC optics model (2a).

If information from other TOTEM detectors (8) is added to information obtained from the RPs detectors then the TOTEM physics reconstruction and analysis (9) can

be done. The physics quantities (cross sections, differential cross sections,...) are reconstructed in this stage. For description of all mentioned modules in details see [11]. One of the quantities which can be reconstructed and further analyzed is proton-proton elastic differential cross section. One of the possible analyzes of elastic differential cross section measured earlier at the ISR will be done in Chapter 4.

2.5 Detectors response

Only a part of the reconstruction chain, as far as the RP track fitting module (6), was used for a particle from the source to see the response of the RP silicon detectors. The study of the response of the RP silicon detectors is one of the first steps towards developing a background suppression algorithm.

To study the response of the detectors we introduce the number N_t of particles with a successfully reconstructed and fitted track ("valid" track) in at least one of the RPs at 147 m or 220 m (each RP station consists of 6 RP units). Similarly we introduce quantity N_h with the same meaning but instead of valid tracks we consider just valid hits.

Some statistics based on successfully reconstructed and fitted tracks ("valid" tracks) for the most important particles (protons, photons, neutrons, electrons, positrons and pions, see Fig. 2.3) are shown in Tab. 2.1. The number N in Tab. 2.1 stands for the number of all particles of a given type, i.e., number of all particles of given type which enter RP147 or RP220 station.

Particle	RP147 station		RP220 station	
	$\frac{N_t}{N}$	$\frac{N_h}{N}$	$\frac{N_t}{N}$	$\frac{N_h}{N}$
p	$\frac{3910}{13060} = 0.30$	$\frac{4183}{13060} = 0.32$	$\frac{3222}{10971} = 0.29$	$\frac{3762}{10971} = 0.34$
γ	$\frac{6643}{341613} = 0.019$	$\frac{47833}{341613} = 0.14$	$\frac{1833}{36547} = 0.05$	$\frac{6461}{36547} = 0.18$
n	$\frac{14}{1705} = 0.0082$	$\frac{223}{1705} = 0.13$	$\frac{9}{591} = 0.015$	$\frac{68}{591} = 0.12$
e^- (e^+)	$\frac{7134}{19231} = 0.37$	$\frac{12751}{19231} = 0.66$	$\frac{232}{3682} = 0.063$	$\frac{1413}{3682} = 0.38$
π^- (π^+)	$\frac{2592}{4880} = 0.53$	$\frac{3316}{4880} = 0.68$	$\frac{127}{253} = 0.50$	$\frac{178}{253} = 0.70$

Table 2.1: Valid tracks and hits at RP147 and RP220. Number N_t (N_h) denotes number of particles of a given type with at least one valid track (hit) at RP147 or RP220. Number N stands for total number of particles with given type entering RP147 or RP220.

We see from Tab. 2.1 that the number of valid hits N_h for proton is nearly the same as the number of valid tracks N_t at both of the RP stations. The same holds also for pions. However, number of valid tracks N_t for electrons (positrons) at RP220 is much less then at RP147; moreover, it is much less then the number of valid hits N_h at RP220. The mean energy of electrons and positrons differs significantly at RP147 (≤ 50 GeV) and at RP220 (few GeV). The energy of protons and pions at RP147 as well as RP220 is generally much higher (up to 7 TeV) than the energy of electrons. Electrons behave in the same manner as positrons and pions with positive charge behave similarly as pions with negative charge, as has been already mentioned in previous sections. On the

contrary, relatively very few neutral particles (photons and neutrons) have at least one valid track (just few percent). The RP silicons detectors detect better charged particles than neutral particles.

Chapter 3

Two-Body Elastic Scattering

This chapter is devoted to the theoretical description of pp (resp. $\bar{p}p$) elastic scattering which is essential for reaching the challenging TOTEM goals. We will present two formulas for complete elastic amplitude $F^{C+N}(s,t)$ which determines elastic differential cross section and takes into account both the Coulomb and hadronic interactions. The first one (historically older) is West and Yennie formula and the second is general formula derived on the basis of eikonal model. We will also introduce the elastic hadron scattering amplitude in the impact parameter space.

3.1 Kinematics

In this thesis, to describe kinematics of particles we will employ commonly used formalism of four-momentum (see [12] or [13])

$$P = (E, \vec{p}) \tag{3.1}$$

where E is total energy of a particle and $\vec{p}$ is its three-momentum. We will use natural units ($\hbar = c = 1$). Scalar product of these four-momentums is defined as follows

$$P^2 = g_{\mu\nu}\, p^\mu p^\nu = E^2 - \vec{p}^2 \tag{3.2}$$

where the metric tensor $g_{\mu\nu}$ is $g_{\mu\nu} = \mathrm{diag}(+1,-1,-1,-1)$ Due to our choice of natural units $\hbar = c = 1$ the energy E and magnitude of $\vec{p}$ (which we will denote by p) have the same units GeV.

A special case of two-body reaction is the elastic scattering

$$1 + 2 \to 1' + 2' \tag{3.3}$$

where the two scattering particles remain in the same state but in a different kinematic configuration. The four-momentum of the ith incoming (outgoing) particle is denoted by P_i (P_i') for $i = 1, 2$ (see Fig. 3.1 in the case of center of mass system CMS).

The kinematics of the given process is fully described by two independent variables. It is possible to choose these two parameters among the three Mandelstam variables, defined as

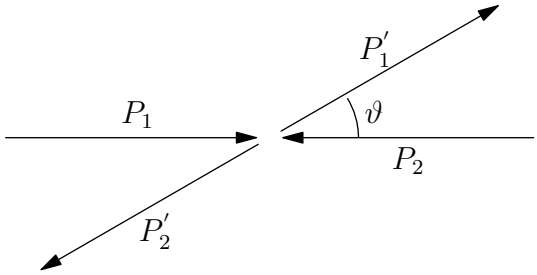

Figure 3.1: Two-body elastic scattering in center of mass system.

$$s = (P_1 + P_2)^2, \tag{3.4}$$
$$t = (P_1 - P_1')^2, \tag{3.5}$$
$$u = (P_1 - P_2')^2. \tag{3.6}$$

We shall use s and t as it is common. It is further convenient to choose center of mass system, because the variable s is the square of the total center of mass energy of colliding particles and the variable t is the squared momentum transfer in this reference frame. In case of pp elastic scattering, which we are interested in, the magnitude of three-momenta of incoming and outgoing particles in CMS are the same (denote them by p, resp. p') and they have equal masses m. The relations between the CMS scattering angle ϑ and three-momentum p (see Fig. 3.1) and variables s and t are

$$s = 4(p^2 + m^2) \tag{3.7}$$

$$t = -2p^2(1 - \cos\,\vartheta). \tag{3.8}$$

We see from the last relation (3.8) that

$$-4p^2 \leq t \leq 0, \tag{3.9}$$

i.e., the value of t is not positive and its minimal value t_{min} is $-4p^2$, in contrast to s which is always positive because it is the total center of mass energy of colliding particles. The value of t_{min} may be expressed also as

$$t_{min} = -s + m^2 \tag{3.10}$$

In high energy limit (i.e., for $s \to \infty$) the mass m can be neglected in formulas (3.7) and (3.10).

In the relativistic theory the elastic differential cross section of two particles may be defined in Mandelstam variables s and t as follows (see [13])

$$\frac{\mathrm{d}\sigma(s,t)}{\mathrm{d}t} = \frac{\pi}{sp^2}\,|F(s,t)|^2 \tag{3.11}$$

where we have introduced scattering amplitude $F(s,t)$ in s and t variables. High-energy elastic scattering of nucleons is realized not only due to the strong interaction but in the case of charged hadrons also as the result of the Coulomb interaction. The Coulomb and nuclear scattering can be characterized by common differential cross section that

may be measured. Elastic differential cross section of charged nucleons is being then currently described with help of a complete elastic scattering amplitude denoted as $F^{C+N}(s,t)$; $F(s,t)$ in Eq. (3.11) being substituted by this amplitude. In the following we will introduce two different formulas of $F^{C+N}(s,t)$, having been used in the past.

3.2 West-Yennie formula

First formula (historically older) of the complete amplitude $F^{C+N}(s,t)$ is commonly written as the sum of hadronic amplitude $F^N(s,t)$ and Coulomb amplitude $F^C(s,t)$ (known from QED) which are mutually bound with the help of relative *real* phase $\alpha\phi(s,t)$ as follows (Bethe formula [14])

$$F^{C+N}(s,t) = F^C(s,t)e^{i\alpha\phi(s,t)} + F^N(s,t) \tag{3.12}$$

where $\alpha = 1/137.036$ is the fine structure constant. The complete amplitude $F^{C+N}(s,t)$ is not, therefore, mere sum of hadronic and Coulomb amplitude. West and Yennie (WY) [15] applying the method of Feynman diagram technique (one photon exchange) derived further in the case of charged point-like particles and of high energy limit (i.e., for $s \to \infty$) for the relative phase function $\phi(s,t)$ the formula being now used in the form

$$\phi(s,t) = \mp\left[\ln\left(\frac{-t}{s}\right) - \int\limits_{-4p^2}^{0} \frac{\mathrm{d}t'}{|t-t'|}\left(1 - \frac{F^N(s,t')}{F^N(s,t)}\right)\right] \tag{3.13}$$

where the upper (lower) sign corresponds to the scattering of nucleons with the same (opposite) charges. It means that at the given energy the t-dependence of the relative phase between the Coulomb and hadronic amplitudes is determined practically by the t-dependent hadronic component $F^N(s,t)$ entering into the integrand of Eq. (3.13). Practically the same result were obtained by Locher [16] at the same time.

Adding two electric form factors $f_1(t)$ and $f_2(t)$ describing the same electric structure of the both colliding hadrons into the Coulomb amplitude one may write

$$F^C(s,t) = \pm\frac{\alpha s}{t} f_1(t) f_2(t). \tag{3.14}$$

The authors of [15] further assumed

(*i*) the influence of spins of all the particles involved may be neglected;

(*ii*) the t-dependence of the modulus of the elastic hadron amplitude is purely exponential in the *whole kinematically allowed region of momentum transfer* t, i.e.,

$$\left|F^N_{WY}(s,t)\right| \sim e^{Bt/2} \tag{3.15}$$

where parameter B is so-called "diffractive slope".

(*iii*) The quantity ρ defined as ratio of the real to imaginary parts of the elastic hadron amplitude is t-independent in the *whole kinematically allowed region of momentum transfer* t.

Only then the mentioned authors were able to calculate integral (3.13) analytically

$$\phi(s,t) = \mp\left[\ln\left(\frac{-Bt}{2}\right) + \gamma\right] \tag{3.16}$$

where $\gamma = 0.577215$ is Euler's constant and derive for the complete amplitude (3.12) the simplified formula

$$F_{WY}^{C+N}(s,t) = \pm\frac{\alpha s}{t} f_1(t) f_2(t) e^{i\alpha\Phi} + \frac{\sigma_{tot}}{4\pi} p\sqrt{s}(\rho + i) e^{Bt/2}. \tag{3.17}$$

which should hold *only* for *small* values of $|t|$. The parameter σ_{tot} is the total nuclear cross section which involves also inelastic interactions. The optical theorem

$$\sigma_{tot}(s) = \frac{4\pi}{p\sqrt{s}} \Im F^N(s, t = 0) \tag{3.18}$$

was also employed to derive the simplified WY formula. The second term on the right hand side of Eq. (3.17) represents the hadronic amplitude $F_{WY}^N(s,t)$.

As to the mentioned assumptions, the first assumption (i) has been discussed in [17] or [18]. According to these papers the spin effects have negligible impact in the case of forward elastic hadron pp scattering in ISR energy range of $\sqrt{s}$, i.e., from 23.5 GeV to 62.5 GeV, and in all high-energy elastic hadron scattering. The first assumption (i) seems, therefore, not to represent practically any important limitation.

On the other hand the second and third assumptions (ii) and (iii) are much more important, see, e.g., [19]. The purely t-dependence of hadronic amplitude $\left|F_{WY}^N(s,t)\right|$ determines according to Eq. (3.11) the corresponding differential cross section $\left.\frac{\mathrm{d}\sigma^N}{\mathrm{d}t}\right|_{WY}$ and approximately corresponds to observed experimental data for the pp elastic scattering at the ISR energies (where the diffractive structure - existence of diffractive minimum - has been experimentally confirmed) only for t running from the forward direction to diffractive minimum. The purely exponential t-dependence can not describe diffractive structure and so it is without any doubt in contradiction to high energy elastic nucleon experimental data.

In the standard analysis of experimental data, the simplified WY formula (defined by Eqs. (3.16) and (3.17)) has been used for the analysis of differential cross section data in the interference region only (i.e., in the case of elastic nucleon scattering for $|t| \lesssim 0.01$ GeV^2 at present high energies). For higher values of $|t|$ it is believed that the influence of Coulomb scattering can be - on the basis of the WY simplified formula - completely neglected and another formulas exhibiting *different* t-dependence of hadronic amplitude $F^N(s,t)$ (non pure exponential dependence of the modulus and non-constant ratio of real to imaginary part of the hadronic amplitude) are commonly used.

Thus, the whole t-dependence of elastic scattering has been described with the help of two quite different formulas, which represents a significant shortage. However, the simplified WY formula represents a greater disadvantage when already the relative phase $\phi(s,t)$ between the Coulomb and hadronic amplitude given by the original integral formula (3.13) is taken already as real; the ratio $\rho(s,t)$ has to be t-independent [20].

We may also define t-dependent diffractive slope by

$$B(s,t) = \frac{\mathrm{d}}{\mathrm{d}t}\left[\ln\frac{\mathrm{d}\sigma^N}{\mathrm{d}t}\right] = \frac{2}{|F^N(s,t)|}\frac{\mathrm{d}}{\mathrm{d}t}\left|F^N(s,t)\right|. \tag{3.19}$$

and t-dependent ratio

$$\rho(s,t) = \frac{\Re F^N(s,t)}{\Im F^N(s,t)}. \tag{3.20}$$

Both the two quantities depend only on the elastic hadronic amplitude $F^N(s,t)$ and so they characterize hadron scattering. They are t-independent in the simplified WY formula where the modulus of hadronic amplitude $\left|F^N_{WY}(s,t)\right|$ is purely exponential and also the ratio of the real to imaginary parts of hadronic amplitude is t-independent (assumptions (ii) and (iii)).

So, if a hadronic amplitude $F^N(s,t)$ has not a purely exponential modulus or a constant ratio of the real to imaginary parts then there is no reason to require for quantities σ_{tot}, $\rho(s,t=0)$ and $B(s,t=0)$ (fully determined by hadron amplitude) the values to be the same as those of parameters σ_{tot}, ρ and B obtained from the simplified WY formula (3.17).

Let as stress again that the theoretical assumptions used in the derivation of simplified WY amplitude $F^{C+N}_{WY}(s,t)$ are not fulfilled by the experimental data and its current application in this way can be hardly justified. And this is one of the reasons why a more general formula removing these discrepancies and valid in the whole kinematically allowed region of momentum transfer t should be used for analysis of the experimental data.

3.3 Elastic amplitude in the eikonal model

Both theoretical as well as experimental deficiencies of models of elastic nucleon scattering based on WY approach may be removed, if one starts from the eikonal model, see [5].

The elastic scattering amplitude may be defined with the help of Fourier-Bessel (FB) transformation according to Glauber [21] or Islam [22, 23] in the eikonal model as

$$F(s,q^2=-t) = \frac{s}{4\pi i}\int_{\Omega_b} \mathrm{d}^2b\; e^{i\vec{q}.\vec{b}}[e^{2i\delta(s,b)}-1] \tag{3.21}$$

where Ω_b represents the two-dimensional Euclidean space of the impact parameter $\vec{b}$, the vector $\vec{q}$ is defined as $\vec{k}-\vec{k'}$ and eikonal $\delta(s,b)$ is proportional to

$$\delta(s,b) \sim \int_b^\infty \frac{V(s,r)r\mathrm{d}r}{\sqrt{r^2-b^2}}. \tag{3.22}$$

Potential $V(s,r)$ corresponds to potential between particles at individual corresponding positions during their motions. Eq. (3.22) holds for energy-dependent spherically symmetric potential $V(s,r)$ that might be generally complex. Due to Eq. (3.21) the complete elastic amplitude $F^{C+N}(s,t)$ of two charged and spinless nucleons is fully determined by the total eikonal $\delta^{C+N}(s,b)$. Taking into account the Eq. (3.22) for eikonal the total eikonal $\delta^{C+N}(s,b)$ is given by the sum of individual eikonals $\delta^C(s,b)$ and $\delta^N(s,b)$ for the Coulomb and hadronic eikonals

$$\delta^{C+N}(s,b) = \delta^C(s,b) + \delta^N(s,b). \tag{3.23}$$

Eq. (3.23) is in agreement with the additivity of potentials, i.e., Coulomb and hadronic potential, and with linearity of potential $V(s,r)$ in expression (3.22). The complete elastic amplitude of charged nucleons in the eikonal model may be thus rewritten as

$$F_{eik}^{C+N}(s,q^2=-t) = \frac{s}{4\pi i}\int\limits_{\Omega_b} \mathrm{d}^2b\; e^{i\vec{q}.\vec{b}}[e^{2i(\delta(s,b)^C+\delta(s,b)^N)}-1] \tag{3.24}$$

The Coulomb and hadronic elastic scattering (the elastic differential cross section) is fully determined by the total eikonal $\delta^{C+N}(s,b)$. Due to Eq. (3.22) the "interference" between the Coulomb and hadronic interactions follows thus from the mere sum of corresponding potentials.

One may further write

$$\begin{aligned} F_{eik}^{C+N}(s,t) &= F^C(s,t)+F^N(s,t)+F^I(s,t) \\ &= F^C(s,t)+F^N(s,t)+\frac{s}{4\pi i}\int\limits_{\Omega_b} \mathrm{d}^2b\; e^{i\vec{q}.\vec{b}}[e^{2i\delta(s,b)^C}-1][e^{2i\delta(s,b)^N}-1] \end{aligned} \tag{3.25}$$

where we have introduced interference term $F^I(s,t)$. We will use this relation in Chapter 4 to show how much important is the interference of the Coulomb and hadron interaction.

According to the authors of [5] it is possible further to derive from Eq. (3.24) for the complete elastic amplitude the following relation

$$F_{eik}^{C+N}(s,t) = \pm\frac{\alpha s}{t}f_1(t)f_2(t)+F^N(s,t)[1\mp i\alpha G(s,t)] \tag{3.26}$$

where

$$G(s,t) = \int\limits_{t_{min}}^{0}\mathrm{d}t'\left\{\ln\left(\frac{t'}{t}\right)\frac{\mathrm{d}}{\mathrm{d}t'}[f_1(t')f_2(t')]-\frac{1}{2\pi}\left[\frac{F^N(s,t')}{F^N(s,t)}-1\right]I(t,t')\right\} \tag{3.27}$$

and

$$I(t,t') = \int\limits_0^{2\pi}\mathrm{d}\Phi''\frac{f_1(t'')f_2(t'')}{t''}; \tag{3.28}$$

here $t''=t+t'+2\sqrt{tt'}\cos\Phi''$. The minimal kinematically allowed value t_{min} in (3.27) equals $-s+4m^2$ (see relation (3.10)). The upper (lower) sign in (3.26) corresponds again to the scattering of particles with the same (opposite) charges. Formulas (3.26), (3.27) and (3.28) should hold generally for *any* s and t with the accuracy up to terms linear in α. This is one of the differences between the general eikonal formula (3.26) and the simplified WY formula defined by Eqs. (3.16) and (3.17) which was derived only for small values of $|t|$. Moreover, the general eikonal formula was derived without any restriction on hadronic amplitude $F^N(s,t)$ (and so the function $G(s,t)$ may be generally complex). The WY formula contains assumption of purely exponential modulus of $F^N(s,t)$ and constant ratio $\rho(s,t)$ of the real to imaginary parts of $F^N(s,t)$, see Section 3.2.

The first term $\frac{\alpha s}{t} f_1(t) f_2(t)$ in Eq. (3.26) is the Coulomb scattering amplitude $F^C(s,t)$ (see Eq. (3.14)). The expression in the last bracket of Eq. (3.26) may be regarded as the first term in the Taylor series expansion of the exponential $e^{\mp i\alpha G}$ and one can write within the same precision

$$F^{C+N}_{eik}(s,t) = F^C(s,t) + F^N(s,t) e^{\mp i\alpha G(s,t)}. \tag{3.29}$$

This formula for complete elastic amplitude is similar to Eq. (3.12) with the relative phase $\phi(s,t)$ between the Coulomb and hadron amplitude. The relative phase $\phi(s,t)$ is taken always as real but the function $G(s,t)$ may be generally complex.

To express proton form factors $f_1(t) = f_2(t)$ in the case of pp or $\bar{p}p$ scattering in the large region of t we can employ t-dependent Borkowski's electric proton form factors

$$f_1(t) = f_2(t) = \sum_{j=1}^{4} \frac{g_j}{w_j - t} \tag{3.30}$$

where parameters g_j and w_j entering into the form factors have been extracted from the measured electron-proton elastic scattering cross sections (see [24]). The integral $I(t,t')$ defined by Eq. (3.28) can be now determined analytically (see [17] or [5]) as follows

$$I(t,t') = \sum_{j,k=1}^{4} g_j g_k W_{jk} I_{jk} \tag{3.31}$$

where for $j \neq k$

$$\begin{aligned} I_{jk} = 2\pi \Bigg[& \frac{(P_j-1)^2}{\sqrt{P_j}(P_j-P_k)(P_j-U)} + \frac{(P_k-1)^2}{\sqrt{P_k}(P_k-P_j)(P_k-U)} + \\ & + \frac{(U-1)^2}{\sqrt{U}(U-P_j)(U-P_k)} \Bigg] \end{aligned} \tag{3.32}$$

and

$$I_{jj} = 2\pi \left[\frac{(P_j-1)(3P_j+P_j^2-U-3P_jU)}{2P_j^{3/2}(P_j-U)^2} + \frac{(U-1)^2}{\sqrt{U}(U-P_j)^2} \right]. \tag{3.33}$$

It holds further that

$$P_j = \frac{w_j + (\sqrt{-t}+\sqrt{-t'})^2}{w_j + (\sqrt{-t}-\sqrt{-t'})^2}, \qquad U = \left(\frac{\sqrt{-t}+\sqrt{-t'}}{\sqrt{-t}-\sqrt{-t'}} \right)^2 \tag{3.34}$$

and

$$W_{jk} = \frac{1}{[w_j + (\sqrt{-t}-\sqrt{-t'})^2][w_k + (\sqrt{-t}-\sqrt{-t'})^2][\sqrt{-t}-\sqrt{-t'}]^2}. \tag{3.35}$$

Formula (3.26) for the complete elastic scattering amplitude is convenient for any t dependence of hadronic amplitude $F^N(s,t)$ without any limitation. It can be either used

for the analysis of differential cross section data at *all* values of t *simultaneously* in a unique way if the hadronic amplitude $F^N(s,t)$ is suitably parametrized. Or, the formula (3.26) can be also used for the determination of the differential cross section data at any values of t if the hadronic amplitude $F^N(s,t)$ is specified within the framework of some phenomenological model description.

In Chapter 4 we will use the general eikonal formula (3.26) for an analysis of two different models of hadronic amplitude $F^N(s,t)$.

3.4 Elastic hadron amplitude and the impact parameter space

The complex hadron scattering amplitude $F^N(s,t)$ can be characterized by two real functions, the modulus $\left|F^N(s,t)\right|$ and the phase $\zeta^N(s,t)$, in this way

$$F^N(s,t) = i\left|F^N(s,t)\right| e^{-i\zeta^N(s,t)}. \tag{3.36}$$

Due to Eqs. (3.36) and (3.20)

$$\tan\zeta^N(s,t) = \rho(s,t). \tag{3.37}$$

This implies that constant quantity $\rho(s,t)$ is equivalent to constant hadronic phase $\zeta^N(s,t)$.

If the hadron amplitude $F^N(s,t)$ is known then the elastic cross section $\sigma_{el}(s)$ may be evaluated with use of the elastic hadronic differential cross section (3.11) ($F(s,t)$ in Eq. (3.11) being substituted by hadronic amplitude $F^N(s,t)$) as

$$\sigma_{el}(s) = \int\limits_{t_{min}}^{0} \frac{\mathrm{d}\sigma^N}{\mathrm{d}t}\mathrm{d}t. \tag{3.38}$$

The inelastic cross section is then defined as

$$\sigma_{inel}(s) = \sigma_{tot}(s) - \sigma_{el}(s). \tag{3.39}$$

where the total cross section is given by the optical theorem (3.18).

To derive distribution of elastic and inelastic collisions in the impact parameter space we may start from the unitarity equation as was done in [25]. According to van Hove [26] the elastic hadron amplitude $F^N(s,t)$ is linked to all production amplitudes $T(s,t,\dots)$ by unitarity condition

$$\Im F^N(s,t) = \frac{p}{4\pi\sqrt{s}}\int \mathrm{d}\Omega' F^{N*}(s,t')F^N(s,t'') + G_{inel}(s,t) \tag{3.40}$$

where

$$\mathrm{d}\Omega' = \sin\vartheta'\mathrm{d}\vartheta'\mathrm{d}\Phi' \tag{3.41}$$

$$t' = 2p\sin\frac{\vartheta'}{2} \tag{3.42}$$

$$t'' = 2p\sin\frac{\vartheta''}{2} \tag{3.43}$$

$$\cos\vartheta'' = \cos\vartheta\cos\vartheta' + \sin\vartheta\sin\vartheta''\cos\Phi'. \tag{3.44}$$

Variables ϑ, ϑ', ... are angels defining the corresponding momentum transfers squared t, t' and t'' in the CMS and $G_{inel}(s,t)$ is the so-called inelastic overlap function representing summation over all possible production (inelastic) states as well as the integration over all other kinematical variables.

The elastic hadron scattering amplitude $h_{el}(s,b)$ in the impact parameter space at *finite* energies may be defined by FB transformation of the elastic hadron scattering amplitude $\left|F^N(s,t)\right|$ (see [23] and [25])

$$\begin{aligned} h_{el}(s,b) &= h_1(s,b) + h_2(s,b) \\ &= \frac{1}{4p\sqrt{s}} \int\limits_{t_{min}}^{0} F^N(s,t) J_0(b\sqrt{-t})\mathrm{d}t + \frac{1}{4p\sqrt{s}} \int\limits_{-\infty}^{t_{min}} \lambda(s,t) J_0(b\sqrt{-t})\mathrm{d}t, \end{aligned} \tag{3.45}$$

where the first term represents the contribution of the FB transformation of $F^N(s,t)$ from the physical region of t and the second one represents the contribution of a complex function $\lambda(s,t)$ in the unphysical region of t. The functions $\lambda(s,t)$ should fulfill some other conditions [22] to guarantee the existence of FB transformation of $F^N(s,t)$ at finite energies. Only the first term is present in Eq. (3.45) in the case of nucleon-nucleon scattering at infinite energies (and $t_{min} = -\infty$), see Eq. (3.10). Function J_0 in Eq. (3.45) is Bessel function of zeroth order which is defined as

$$J_0(x) = \frac{1}{2\pi} \int\limits_{0}^{2\pi} e^{ixcos\varphi}\mathrm{d}\varphi. \tag{3.46}$$

Similarly, the inelastic overlap function in the impact parameter space may equal

$$g_{inel}(s,b) = g_1(s,b) + g_2(s,b), \tag{3.47}$$

where $g_1(s,b)$ is the contribution of the FB transformation of inelastic overlap function $G_{inel}(s,b)$ from the physical region of t and $g_2(s,b)$ represents the contribution from unknown real function $\mu(s,t) = G_{inel}(s,t)$ in the unphysical region of t. Similarly as in the case of function $\lambda(s,t)$, the functions $\mu(s,t)$ should fulfill also some other conditions to guarantee the existence of FB transformation of $G_{inel}(s,t)$ at finite energies. The unitarity equation (3.40) in the impact parameter space can be further rewritten as

$$\Im h_1(s,b) = |h_1(s,b)|^2 + g_1(s,b) + K(s,b), \tag{3.48}$$

where

$$\begin{aligned} K(s,b) = \frac{1}{16\pi^2 s} &\int\limits_{tmin}^{0} \mathrm{d}t_1 \int\limits_{tmin}^{0} \mathrm{d}t_2 F^{N*}(s,t_2) F^N(s,t_1) \\ &\times \left[J_0\left(\frac{b}{2p}\sqrt{-t_1(4p^2+t_2)}\right) J_0\left(\frac{b}{2p}\sqrt{-t_2(4p^2+t_1)}\right) - J_0(b\sqrt{-t_1}) J_0(b\sqrt{-t_2}) \right]. \end{aligned} \tag{3.49}$$

The correction function $K(s,b)$ vanishes at $b = 0$ and $b \to \infty$. It holds further

$$\int_0^\infty b\mathrm{d}b\ \Im h_2(s,b) = \int_0^\infty b\mathrm{d}b\ g_2(s,b) = \int_0^\infty b\mathrm{d}b\ K(s,b) = 0. \tag{3.50}$$

Only the non-negative function $|h_1(s,b)|^2$ in Eq. (3.48) is standardly interpreted as distribution function of elastic processes in the impact parameter space (so-called elastic profile function). The other two functions $\Im h_1(s,b)$ and $g_1(s,b)$ may be negative for some values of b and so they can not be interpreted as distribution function of any process. However, the integrals of the functions $\Im h_1(s,b)$, $|h_1(s,b)|^2$ or $g_1(s,b)$ over all possible impact parameter values represent the total, elastic and inelastic cross sections [22]. One may ask whether it is possible to modify Eq. (3.48) so that it has a form

$$h_{tot}(s,b) = |h_1(s,b)|^2 + g_{inel}(s,b), \tag{3.51}$$

where $h_{tot}(s,b)$ ($g_{inel}(s,b)$) is distribution function of total (inelastic) processes in the impact parameter space. It must hold

$$8\pi \int_0^\infty b\mathrm{d}b\ h_{tot}(s,b) = \sigma_{tot}(s) \tag{3.52}$$

and

$$\frac{8\pi}{\sigma_{tot}} \int_0^\infty b\mathrm{d}b\ b^2 h_{tot}(s,b) = \langle b^2(s)\rangle_{tot}. \tag{3.53}$$

The total mean-square $\langle b^2(s)\rangle_{tot}$ will be defined in the following. To obtain Eq. (3.51) we may introduce a real function $c(s,b)$ in the impact parameter space, add this function to the both sides of Eq. (3.48) so that

$$h_{tot}(s,b) = \Im h_1(s,b) + c(s,b), \tag{3.54}$$

$$g_{inel}(s,b) = g_1(s,b) + K(s,b) + c(s,b). \tag{3.55}$$

The real function $c(s,b)$ can not be an arbitrary function but it must fulfill following conditions and requirements

1. it should bring both the function $h_{tot}(s,b)$ (and also $g_{inel}(s,b)$) to be non negative for all values of b;

2. it must preserve the value of total cross section $\sigma_{tot}(s)$ in Eq. (3.52), i.e., it must hold $\int_0^\infty b\mathrm{d}b\ c(s,b) = 0$;

3. and similarly it must not change the value of $\langle b^2(s)\rangle_{tot}$, i.e., it must hold $\int_0^\infty b\mathrm{d}b\ b^2 c(s,b) = 0$.

If the distribution of elastic processes $|h_1(s,b)|^2$ has (for given s value) its maximum at impact parameter $b = 0$, i.e., for head-on collisions of two particles, we speak about "central" behavior of elastic collision. In the case when this distribution has maximum

at some $b > 0$ we denote this situation as "peripheral" behavior of elastic collision. The given behavior depends mainly on the t-dependence of phase $\zeta^N(s,t)$.

If the distribution function of total, elastic and inelastic collisions in the impact parameter are known then one may evaluate mean-squares of impact parameter for corresponding processes. We may define mean-square of the impact parameter in the case of elastic processes as

$$\langle b^2(s)\rangle_{el} = \frac{\int\limits_0^\infty bdb\; b^2\,|h_1(s,b)|^2}{\int\limits_0^\infty bdb\;|h_1(s,b)|^2}. \tag{3.56}$$

Similarly, we may define $\langle b^2(s)\rangle_{tot}$ and $\langle b^2(s)\rangle_{inel}$ in the case of total and inelastic collisions. Moreover, according to [25] the mean-squares of all the processes may be derived directly from the t-dependent elastic hadron amplitude $F^N(s,t)$ without trying establish the whole profiles.

The elastic mean-square $\langle b^2(s)\rangle_{el}$ defined by (3.56) can be rewritten as a sum of two terms

$$\begin{aligned}\langle b^2(s)\rangle_{el} &= \langle b^2(s)\rangle_{mod} + \langle b^2(s)\rangle_{ph} \\ &= \frac{4\int\limits_{t_{min}}^0 \mathrm{d}t|t|\left(\frac{\mathrm{d}}{\mathrm{d}t}\left|F^N(s,t)\right|\right)^2}{\int\limits_{t_{min}}^0 \mathrm{d}t\,|F^N(s,t)|^2} + \frac{4\int\limits_{t_{min}}^0 \mathrm{d}t\left|F^N(s,t)\right|^2|t|\left(\frac{\mathrm{d}}{\mathrm{d}t}\zeta^N(s,t)\right)}{\int\limits_{t_{min}}^0 \mathrm{d}t\,|F^N(s,t)|^2}\end{aligned} \tag{3.57}$$

where the contributions of the modulus and of the phase are separated and both are non-negative. The first term $\langle b^2(s)\rangle_{mod}$ may be derived using only the modulus of the hadronic amplitude $F^N(s,t)$ while the second term $\langle b^2(s)\rangle_{ph}$ is influenced also by the hadronic phase $\zeta^N(s,t)$.

Similarly, the total mean-square $\langle b^2(s)\rangle_{tot}$ can be evaluated with use of $F^N(s,t)$ as

$$\langle b^2(s)\rangle_{tot} = 4\left(\frac{\frac{d}{dt}\left|F^N(s,t)\right|}{|F^N(s,t)|} - \tan\zeta^N(s,t)\frac{d}{dt}\zeta^N(s,t)\right)\Bigg|_{t=0}. \tag{3.58}$$

To derive $\langle b^2(s)\rangle_{inel}$ we may multiply unitarity equation (3.51) by b^3 and integrate over all possible impact parameter values b:

$$\int\limits_0^\infty bdb\; b^2 h_{tot}(s,b) = \int\limits_0^\infty bdb\; b^2\,|h_1(s,b)|^2 + \int\limits_0^\infty bdb\; b^2 g_{inel}(s,b). \tag{3.59}$$

Taking into account definitions of corresponding $\langle b^2(s)\rangle$ and the fact that integrals of distribution function over all possible values of b represent corresponding cross section one can further obtain

$$\sigma_{tot}(s)\langle b^2(s)\rangle_{tot} = \sigma_{el}(s)\langle b^2(s)\rangle_{el} + \sigma_{inel}(s)\langle b^2(s)\rangle_{inel}. \tag{3.60}$$

The cross sections σ_{el}, σ_{tot} and σ_{inel} as well as mean-squares $\langle b^2(s)\rangle_{tot}$ and $\langle b^2(s)\rangle_{el}$ in Eq. (3.60) are derived using only the hadron amplitude $F^N(s,t)$, see Eqs. (3.38), (3.18),

(3.39), (3.58) and (3.57). Eq. (3.60) allows, therefore, to evaluate also $\langle b^2(s)\rangle_{inel}$ on the basis of $F^N(s,t)$.

Moreover, all terms in Eq. (3.60) are positive, and so one can derive also the following upper bounds of mean squares of impact parameters for elastic and inelastic processes:

$$\langle b^2(s)\rangle_{el} \leq \langle b^2(s)\rangle_{tot} \frac{\sigma_{tot}(s)}{\sigma_{el}(s)} \equiv \langle b^2(s)\rangle_{el}^{bound}; \tag{3.61}$$

$$\langle b^2(s)\rangle_{inel} \leq \langle b^2(s)\rangle_{tot} \frac{\sigma_{tot}(s)}{\sigma_{inel}(s)} \equiv \langle b^2(s)\rangle_{inel}^{bound}. \tag{3.62}$$

As it follows from the experiment $\sigma_{el} < \sigma_{inel}$ the bound for elastic processes is much higher than that for inelastic ones.

3.5 Luminosity at the LHC

The luminosity $\mathcal{L}$ is a constant quantity which in elastic processes bounds together a differential counting rate $\frac{\mathrm{d}N_{el}^{C+N}}{\mathrm{d}t}$, the number of counts $\mathrm{d}N_{el}$ per unit of time in a small interval around momentum transfer $\mathrm{d}t$ divided by $\mathrm{d}t$, with the corresponding complete elastic differential cross section

$$\frac{\mathrm{d}N_{el}^{C+N}}{\mathrm{d}t} = \mathcal{L}\frac{\mathrm{d}\sigma}{\mathrm{d}t}. \tag{3.63}$$

The normalization factor (factor of proportionality) $\mathcal{L}$ has units of $(\text{area})^{-1}(\text{time})^{-1}$. The luminosity $\mathcal{L}$ is one of the basic parameters of every accelerator which describes how effectively the accelerator performs. Experimentally, the luminosity at the LHC is planed to be determined at the t lying inside the interference region $6 \times 10^{-4}\text{GeV}^2 < |t| < 10^{-3}\text{GeV}^2$ where both the Coulomb and hadron interactions have to be taken into account.

The elastic differential cross section $\frac{\mathrm{d}\sigma^{C+N}}{\mathrm{d}t}$ defined by Eq. (3.11) is determined with the help of the complete elastic scattering amplitude $F^{C+N}(s,t)$, which can be calculated at small values of t either according to the WY simplified approach or by the eikonal more precise approach.

To measure σ_{tot} and the luminosity $\mathcal{L}$ simultaneously TOTEM plans to take also the advantage of optical theorem (3.18), see [7]:

$$\mathcal{L}\sigma_{tot}^2 = \frac{16\pi}{1+\rho^2(s,t=0)} \left.\frac{\mathrm{d}N_{el}}{\mathrm{d}t}\right|_{t=0} \tag{3.64}$$

With additional relation

$$\mathcal{L}\sigma_{tot} = N_{el} + N_{inel} \tag{3.65}$$

one obtains a system of 2 equations which can be solved for σ_{tot} and $\mathcal{L}$ independently of each other:

$$\sigma_{tot} = \frac{16\pi}{1+\rho^2} \frac{\left.\frac{\mathrm{d}N_{el}}{\mathrm{d}t}\right|_{t=0}}{N_{el}+N_{inel}}, \tag{3.66}$$

$$L = \frac{1+\rho^2}{16\pi} \frac{(N_{el}+N_{inel})^2}{\left.\frac{\mathrm{d}N_{el}}{\mathrm{d}t}\right|_{t=0}} \tag{3.67}$$

Hence the quantities to be measured or taken from external theoretical predictions are the following:

- **The inelastic rate** N_{inel} consisting of non-diffractive minimum bias events ($\sim$ 65 mb at LHC) and diffractive events ($\sim$ 18 mb at LHC) which will be measured by TOTEM inelastic telescopes T1 and T2.
- **The total nuclear elastic rate** N_{el} measured by the Roman Pot System.
- **The nuclear part of the differential counting rate extrapolated to** $t = 0$, i.e., $\left.\frac{\mathrm{d}N_{el}}{\mathrm{d}t}\right|_{t=0}$.
- **Quantity** $\rho(s,t)$ extrapolated to $t = 0$.

Chapter 4

Analysis of experimental data

In this chapter, we will analyze and discuss some consequences of two phenomenological models of hadronic amplitude $F^N(s,t)$, that have been used already earlier. Because there is not any reliable theory of elastic processes, the only way how to establish the hadronic amplitude is to parameterize it and then fit it to measured data. The model with constant hadronic phase and that proposed by Brazil group will be discussed. We shall go back to pp (resp. $\bar{p}p$) experimental data obtained earlier at energy of 52.8 GeV (resp. 541 GeV) that is represented by the measured elastic differential cross section $\frac{\mathrm{d}\sigma(s,t)}{\mathrm{d}t}$. To demonstrate some consequences of choice of hadronic amplitude $F^N(s,t)$ the newly developed program (as already mentioned) written in C++ will be made use of. It is used in fitting a hadronic amplitude $F^N(s,t)$ to measured pp or $\bar{p}p$ elastic differential cross sections at given energies with use of the eikonal formula (3.26) for the complete amplitude $F_{eik}^{C+N}(s,t)$ and computes some other physically significant quantities introduced in previous chapter.

4.1 Model of hadronic amplitude with constant hadronic phase

The assumption of constant (t-independent) quantity $\rho(s,t)$ (see definition (3.20)) in the whole region of kinematically allowed values of t is contained in the simplified WY formula (3.17) for complete amplitude $F_{WY}^{C+N}(s,t)$ (see Section 3.2). However, this assumption can not be tested with the use of simplified WY formula, because this formula may hold only for very small values of $|t|$. In the following we shall use the eikonal formula (3.26) for the complete amplitude $F_{eik}^{C+N}(s,t)$ which is valid in the whole region of kinematically allowed values of t and we shall test the assumption of constant quantity $\rho(s,t)$.

The aim will be to find out whether it is possible to fit measured elastic differential cross section under the assumption of constant quantity $\rho(s,t)$ and to show also the consequences in the impact parameter space (see Section 3.4) of this assumption.

We will denote the corresponding nuclear amplitude by $F_A^N(s,t)$. Since the hadronic amplitude $F^N(s,t)$ is complex function we may parameterize two real functions, the phase $\zeta^N(s,t)$ and the modulus $\left|F^N(s,t)\right|$, see Eq. (3.36), or real $\Re F^N(s,t)$ and imaginary $\Im F^N(s,t)$ part of the hadronic amplitude. Both approaches are equivalent.

Due to Eq. (3.37) we may express the phase $\zeta_A^N(s,t)$ corresponding to hadronic amplitude $F_A^N(s,t)$ as

$$\zeta_A^N(s,t) = \zeta_0 \tag{4.1}$$

where ζ_0 is a free parameter. The modulus of hadronic amplitude $\left|F_A^N(s,t)\right|$ may be parametrized as

$$\left|F_A^N(s,t)\right| = (a_1 + a_2 t)e^{b_1 t + b_2 t^2 + b_3 t^3} + (c_1 + c_2 t)e^{d_1 t + d_2 t^2 + d_3 t^3}. \tag{4.2}$$

This choice of the parameterization of $\left|F_A^N(s,t)\right|$ was used already in [5] and it is sufficiently flexible to describe measured differential cross section.

We will perform two fits, denoted by Fit A_1 and Fit A_2, of the hadronic amplitude $F_A^N(s,t)$ to experimental data. All the free parameters of $F_A^N(s,t)$ will be fitted to experimental data represented by elastic differential cross section for pp scattering at energy of 52.8 GeV (Fit A_1) and also for $\bar{p}p$ scattering at energy of 541 GeV (Fit A_2) so that both the Coulomb and hadronic interaction will be taken into account.

4.2 Brazil model of hadronic amplitude

The second phenomenological model of $F^N(s,t)$, which we will denote by $F_B^N(s,t)$, was proposed by Brazil group in [27] where the real and imaginary part of the hadronic amplitude was parameterized in the case of pp scattering at energy of $\sqrt{s} = 52.8$ GeV as

$$\Re F_B^N(s,t) = \mu \sum_{j=1}^{2} \alpha_j e^{\beta_j t} \tag{4.3}$$

$$\Im F_B^N(s,t) = \sum_{j=1}^{5} \alpha_j e^{\beta_j t} \tag{4.4}$$

where

$$\mu = \frac{\rho(s,t=0)}{\alpha_1 + \alpha_2} \sum_{j=1}^{5} \alpha_j. \tag{4.5}$$

The parameters α_j and β_j are real free parameters. The parameter $\rho(s,t=0)$ at energy of $\sqrt{s} = 52.8$ GeV equals 0.078 in [27] and it really corresponds to the ratio of $\Re F_B^N(s,t)$ to $\Im F_B^N(s,t)$ at $t = 0$. Very similar parameterization is possible to find also in [28].

The value 0.078 of the parameter $\rho(s,t=0)$ was determined on the basis of the simplified WY formula, i.e., under the assumptions that both the quantities $B(s,t)$ and $\rho(s,t)$ in the whole region of kinematically allowed values of t are constant (t-independent), see definitions (3.19) and (3.20). However, both quantities $B(s,t)$ and $\rho(s,t)$ corresponding to the hadronic amplitude $F_B^N(s,t)$ are t-dependent (non-constant) and so there is no reason to require the value of $\rho(s,t=0)$ to be 0.078.

Moreover, the authors of [27] selected the differential cross section data above the region of $-t > 0.01$ GeV^2 and neglected possible influence of Coulomb interaction at higher values of $|t|$. We will use the differential cross section data also for $-t < 0.01$ and employ interference formula (3.26) to take also the Coulomb interaction into account, see next section.

We will present a fit, denoted by Fit B, of the hadronic amplitude $F_A^N(s,t)$ to measured elastic differential cross section at energy of $\sqrt{s} = 52.8$ GeV and the aim will be to take also the Coulomb interaction in to account and to show some consequences in the impact parameter space, similarly as in the case of previous model of the hadronic amplitude $F_A^N(s,t)$.

4.3 Fitting procedure

To perform all the three fits mentioned in the two previous sections and to take both the Coulomb and hadronic interaction into account for all values of t we will start from formula (see Eq. (3.11))

$$\left.\frac{\mathrm{d}\sigma(s,t)}{\mathrm{d}t}\right|_{eik} = C_{norm}\frac{\pi}{sp^2}\left|F_{eik}^{C+N}(s,t)\right|^2 \tag{4.6}$$

where the formula (3.26) for the complete elastic amplitude $F_{eik}^{C+N}(s,t)$ (in eikonal approach) will be applied to. The parameter C_{norm} corresponds to one percent systematic error of measured cross section and it will be newly fitted within the bounds from 0.99 to 1.01 in the case of pp scattering at energy of $\sqrt{s} = 52.8$ GeV. In the case of $\bar{p}p$ at energy of $\sqrt{s} = 541$ GeV it will be fixed at value $C_{norm} = 1$.

To determine function $F_{eik}^{C+N}(s,t)$ we shall use t-dependent Borkowski's electric proton form factors (3.30), with parameters g_j and w_j taken from [24], for the form factors $f_1(t) = f_2(t)$ involved in Eq. (3.26). The integral $I(t,t')$ in (3.26) will be analytically computed with use of formula (3.31). Now, if we have expression for proton form factors, we may employ one of the models of hadronic amplitude $F_A^N(s,t)$ or $F_B^N(s,t)$ and so fully determine the r.h.s. of Eq. (3.26) for the complete amplitude $F_{eik}^{C+N}(s,t)$, i.e., elastic differential cross section $\left.\frac{\mathrm{d}\sigma(s,t)}{\mathrm{d}t}\right|_{eik}$.

We will analyze and discuss the fits of pp experimental data of the measured elastic differential cross section $\frac{\mathrm{d}\sigma(s,t)}{\mathrm{d}t}$ in region of $-t$ from 0.00126 GeV^2 to 9.75 GeV^2 (243 points) taken from [29] and [30]. We will also discuss $\bar{p}p$ elastic differential cross section in region of $-t$ from 0.000875 GeV^2 to 2.13 GeV^2 (227 points) taken from [31].

As the experimental $\bar{p}p$ differential cross section at energy of 541 GeV was measured in different experiments and at different partially overlapping momentum transfer regions they had to be properly normalized. Corresponding normalization factors have been introduced as additional free parameters and in the final stage of optimization they were taken as constants. The overall normalization factor was then determined from the normalization condition

$$\sigma_{tot}(1+\rho^2) = (63.3 \pm 1.5)\ \mathrm{mb} \tag{4.7}$$

which was used also in [5].

All the free parameters of $F_A^N(s,t)$ will be fitted to elastic differential cross section $\frac{\mathrm{d}\sigma(s,t)}{\mathrm{d}t}$ for pp scattering at energy of 52.8 GeV (Fit A_1) and also for $\bar{p}p$ scattering at energy of 541 GeV (Fit A_2). The t-dependence of $\left|F_A^N(s,t)\right|$ (see (4.2)) is extrapolated with a constant positive value of a slope at momentum transfer lower then -9.75 GeV^2 in the case of pp data and -2.13 GeV^2 for $\bar{p}p$ data to suppress raising of the modulus for grater values of $|t|$. Practically the same results presented in next sections may be obtained also with constant extrapolation, so the value of this slope is not essential.

To fit all the free parameters of $F_B^N(s,t)$ the values of free parameters taken from [27] were used as initial values and fitted to experimental data with the use of interference formula (3.26) for $F_{eik}^{C+N}(s,t)$ (Fit B). We use normalization $\frac{\mathrm{d}\sigma^N}{\mathrm{d}t} = \pi \left|F_B^N(s,t)\right|^2$ for $F_B^N(s,t)$. This normalization differs from normalization of $F_A^N(s,t)$ ($\frac{\mathrm{d}\sigma^N}{\mathrm{d}t} = \frac{\pi}{sp^2}\left|F_A^N(s,t)\right|^2$, see Eq. (3.11)) but it is the same as in [27].

To perform all the three fits new program written in C++ was developed. It is used in fitting a hadronic amplitude $F^N(s,t)$ to measured pp or $\bar{p}p$ elastic differential cross section at given energy with use of Eq. (4.6) and computes some other physically significant quantities. This new program re-implements many functions from FORTRAN programs developed in Ref. [5] in an object-oriented way and so its functionality may be easily extended. The numerical precision of the new C++ program is comparable to the FORTRAN programs. It uses ROOT libraries [10] and may be implemented also in the TOTEM software as a part of analysis module, see module (9) in Fig. 2.6.

The numerical minimization of the chi-square (χ^2) values has been performed in all cases with the help of the Minuit2 minimization package [32] which is part of ROOT [10]. Minuit2 is a new object-oriented implementation, written in C++, of the popular FORTRAN MINUIT minimization package [33]. The corresponding statistical errors of the free parameters were determined by the HESSE procedure (class ROOT::Minuit2::MnHesse).

In the following sections we will present new results of the fitting of the two phenomenological models of the elastic hadronic amplitude $F_A^N(s,t)$ and $F_B^N(s,t)$ presented in previous section.

4.4 Differential cross section

Values of all fitted parameters of the hadronic amplitude $F_A^N(s,t)$ in the case of pp (Fit A_1) and $\bar{p}p$ (Fit A_2) differential cross sections can be found in Tab. 4.1. In the case of Fit A_2 we have put $a_2 = c_2 = 0$. Similarly, values of all fitted parameters of $F_B^N(s,t)$ (Fit B) are in Tab. 4.2.

The elastic differential cross section corresponding to Fit A_1, Fit A_2 or Fit B is plotted in Fig. 4.1. Hadronic elastic differential cross section given by just the corresponding hadronic amplitude $F_A^N(s,t)$ or $F_B^N(s,t)$, see Eq. (3.11), is for higher values of t practically the same as the complete elastic differential cross sections for all the fits.

It is possible to fit both pp and $\bar{p}p$ experimental differential cross section at energy of 52.8 GeV, resp. 541 GeV, by hadronic amplitude $F_A^N(s,t)$ (Fit A_1 and Fit A_2), i.e., under the assumption of constant quantity $\rho(s,t)$. In the case of Fit B (at energy of 52.8 GeV) the value of corresponding reduced chi-square χ^2/DOF (total chi-square divided by number of degrees of freedom) is smaller than for Fit A_1, even thought the complete elastic differential cross section seems to differ significantly at $-t > 9$ GeV^2.

Fits very similar to Fit A_1 and Fit A_2 with the same parameterization (4.2) of the modulus of hadronic amplitude $F^N(s,t)$ but with different parameterization of hadronic phase $\zeta^N(s,t)$ have been done in [5]. The phase $\zeta^N(s,t)$ was parameterized in [5] as

$$\zeta^N(s,t) = \zeta_0 + \zeta_1 \left|\frac{t}{t_0}\right|^{\kappa} e^{\nu t} + \zeta_2 \left|\frac{t}{t_0}\right|^{\lambda} \tag{4.8}$$

in "general phase" (without any restriction), or as

$$\zeta^N(s,t) = \arctan \frac{\rho_0}{1 - \left|\frac{t}{t_{diff}}\right|} \tag{4.9}$$

where t_{diff} corresponds to a diffractive minimum (so-called "standard phase"). The values of χ^2/DOF corresponding to Fit A_1 and Fit A_2 with constant phase are grater then the values of χ^2/DOF corresponding to the analogous fits in [5] with general and standard phase (both t-dependent). The only exception is the value of χ^2/DOF corresponding to Fit A_2 which is comparable to the analogous fit with standard phase. Neither of the parameterizations $F_A^N(s,t)$ or $F_B^N(s,t)$ give better χ^2/DOF than the parameterization in general case introduced in [5].

		Fit A_1	Fit A_2
Data		pp	$\bar{p}p$
$F^N(s,t)$		$F_A^N(s,t)$	$F_A^N(s,t)$
$\sqrt{s}$	[GeV]	52.8	541
C_{norm}		0.996 ± 0.013	1
ζ_0		0.0648 ± 0.0051	0.1128 ± 0.0066
a_1		12139 ± 56	1888000 ± 2800
a_2	[GeV^{-2}]	10800 ± 100	0
b_1	[GeV^{-2}]	5.787 ± 0.020	8.234 ± 0.036
b_2	[GeV^{-4}]	3.130 ± 0.054	4.89 ± 0.16
b_3	[GeV^{-6}]	1.329 ± 0.036	5.11 ± 0.20
c_1		60.9 ± 9.9	3.05 ± 0.52
c_2	[GeV^{-2}]	-0.4 ± 5.8	0
d_1	[GeV^{-2}]	0.837 ± 0.063	-15.33 ± 0.25
d_2	[GeV^{-4}]	-0.0430 ± 0.031	-10.10 ± 0.19
d_3	[GeV^{-6}]	-0.0056 ± 0.0024	-2.001 ± 0.062
χ^2/DOF		673.316/231	279.927/218

Table 4.1: Values of free parameters in $F_A^N(s,t)$, Fit A_1 and Fit A_2. Symbol χ^2/DOF means total chi-square divided by number of degrees of freedom.

		Fit B
Data		pp
$F^N(s,t)$		$F_B^N(s,t)$
$\sqrt{s}$	[GeV]	52.8
$\rho(s,t=0)$		0.078
C_{norm}		0.994 ± 0.011
α_1	[GeV^{-2}]	-0.02133 ± 0.00079
α_2	[GeV^{-2}]	1.130 ± 0.028
α_3	[GeV^{-2}]	3.665 ± 0.016
α_4	[GeV^{-2}]	-3.062 ± 0.015
α_5	[GeV^{-2}]	7.041 ± 0.024
β_1	[GeV^{-2}]	0.7971 ± 0.0083
β_2	[GeV^{-2}]	17.04 ± 0.39
β_3	[GeV^{-2}]	2.2763 ± 0.0043
β_4	[GeV^{-2}]	2.1628 ± 0.0041
β_5	[GeV^{-2}]	5.771 ± 0.021
χ^2/DOF		484.391/232

Table 4.2: Values of free parameters in $F_B^N(s,t)$, Fit B. Values of free parameters in $F_B^N(s,t)$ at energy of 52.8 GeV. Symbol χ^2/DOF means total chi-square divided by number of degrees of freedom.

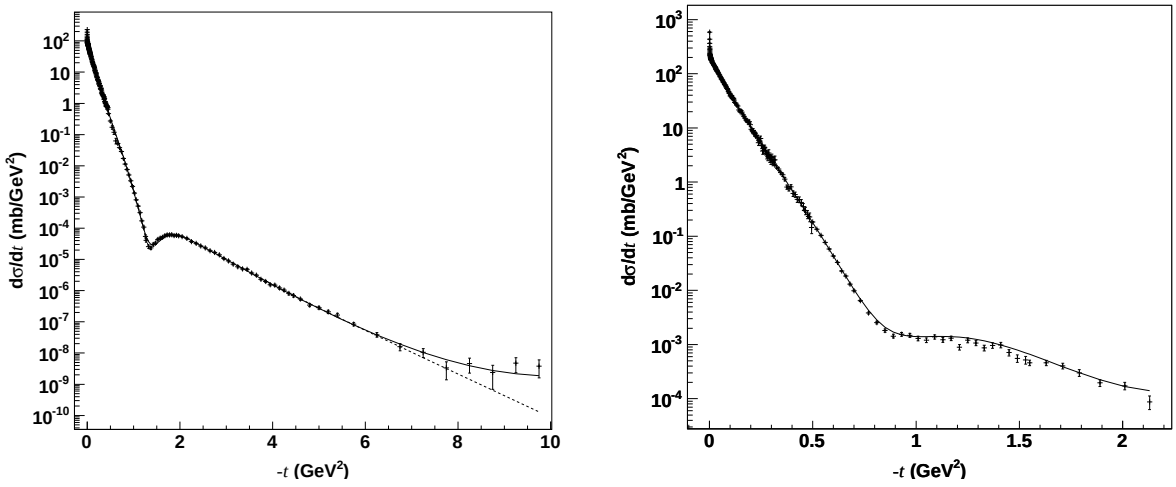

(a) solid line - Fit A_1; dashed line - Fit B

(b) Fit A_2 ($F_A^N(s,t)$, $\bar{p}p$, $\sqrt{s}$ = 541 GeV)

Figure 4.1: Complete elastic differential cross section corresponding to (a) Fit A_1 ($F_A^N(s,t)$, pp, $\sqrt{s}$ = 52.8 GeV), Fit B ($F_B^N(s,t)$, pp, $\sqrt{s}$ = 52.8 GeV) and (b) Fit A_2.

4.5 Interference between the Coulomb and hadron scattering

To show how much important is the interference of the Coulomb and hadron interaction we may use Eq. (3.25) with interference term $F^I(s,t)$. The importance of this term for elastic differential cross section given by Eq. (4.6) may be represented by fraction

$$f(s,t) = \frac{\left|F^{C+N}_{eik}(s,t)\right|^2 - \left|F^C(s,t)\right|^2 - \left|F^N(s,t)\right|^2}{\left|F^N(s,t)\right|^2}. \tag{4.10}$$

This fraction is plotted in Fig. 4.2 and is not negligible also around diffractive dip in the case of Fit A_2 and Fit B. This is characteristic also for many other models of hadronic amplitude $F^N(s,t)$, not only for the models $F^N_A(s,t)$ and $F^N_B(s,t)$ (see, e.g., [5]). The neglection of the Coulomb interaction for higher values of $|t|$ can be, therefore, in the case of same models not straightforward.

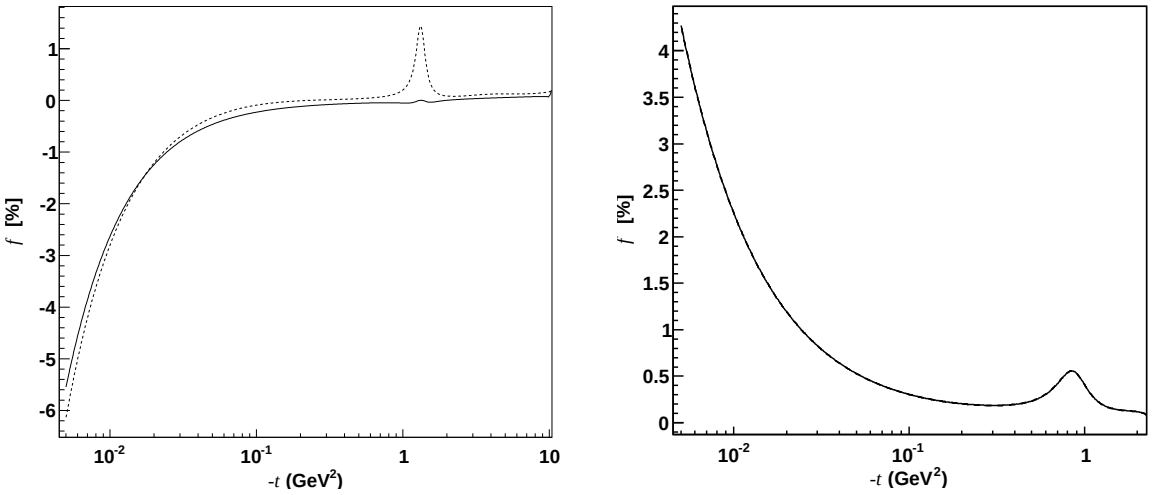

(a) solid line - Fit A_1; dashed line - Fit B

(b) Fit A_2

Figure 4.2: Interference ratio $f(s,t)$ given by Eq. (4.10). (a) solid line corresponds to Fit A_1 ($F^N_A(s,t)$, pp, $\sqrt{s} = 52.8$ GeV) and dashed line corresponds to Fit B ($F^N_B(s,t)$, pp, $\sqrt{s} = 52.8$ GeV). (b) Fit A_2 ($F^N_A(s,t)$, $\bar{p}p$, $\sqrt{s} = 541$ GeV).

4.6 Quantities B and ρ

If we compare Fit A_1 and Fit B both at the same energy of $\sqrt{s} = 52.8$ GeV, we see that the corresponding t-dependent diffractive slopes $B(s,t)$, i.e., the hadronic moduluses $\left|F^N(s,t)\right|$ (see definition (3.19)) are similar, see Figs. 4.3 and 4.4. The corresponding hadronic phases $\zeta^N(s,t)$ differ significantly - one phase is constant (Fit A_1) and the second one is t-dependent (Fit B), see Fig. 4.5. However, the change in the interval $-t \in (0, 0.8\text{GeV}^2)$ is practically negligible, a stronger change begins only at $-t \approx 0.8$ GeV and can not influence the value of root-mean-square of elastic profile $\sqrt{\langle b^2(s)\rangle_{el}}$, see Section 4.8. The dashed lines delimit the values of exhibited quantities within the statistical errors.

The hadronic modulus $\left|F^N(s,t)\right|$ influences much more significantly the value of $\frac{\mathrm{d}\sigma}{\mathrm{d}t}$, and so the value of χ^2, than the hadronic phase $\zeta^N(s,t)$. This fact is also known from [5].

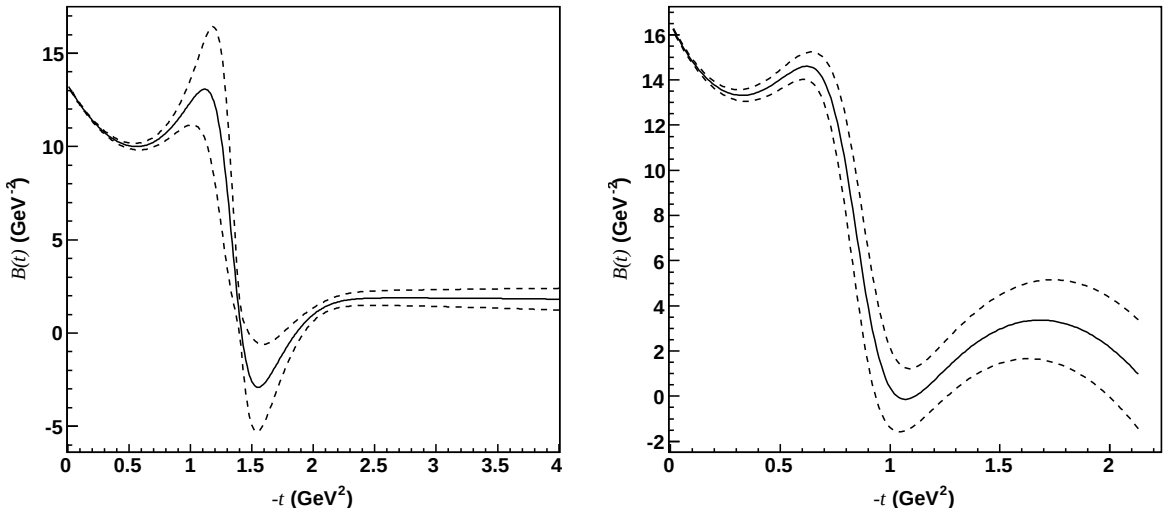

(a) Fit A_1 ($F_A^N(s,t)$, pp, $\sqrt{s} = 52.8$ GeV) (b) Fit A_2 ($F_A^N(s,t)$, $\bar{p}p$, $\sqrt{s} = 541$ GeV)

Figure 4.3: Diffractive slope $B(s,t)$ given by Eq. (3.19) and corresponding to (a) Fit A_1 and (b) Fit A_2.

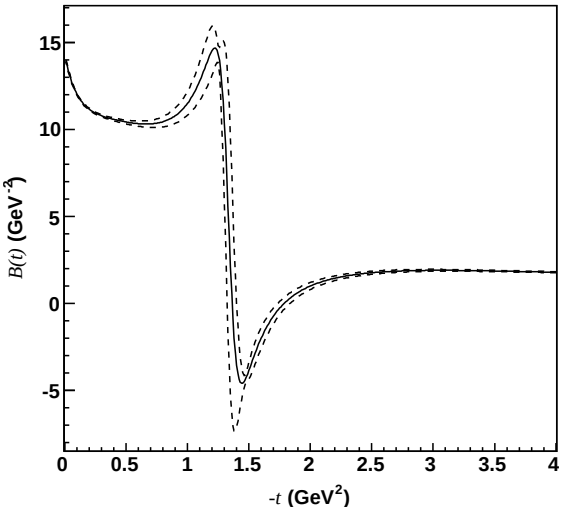

Figure 4.4: Diffractive slope $B(s,t)$ given by Eq. (3.19) and corresponding to Fit B ($F_B^N(s,t)$, pp, $\sqrt{s} = 52.8$ GeV).

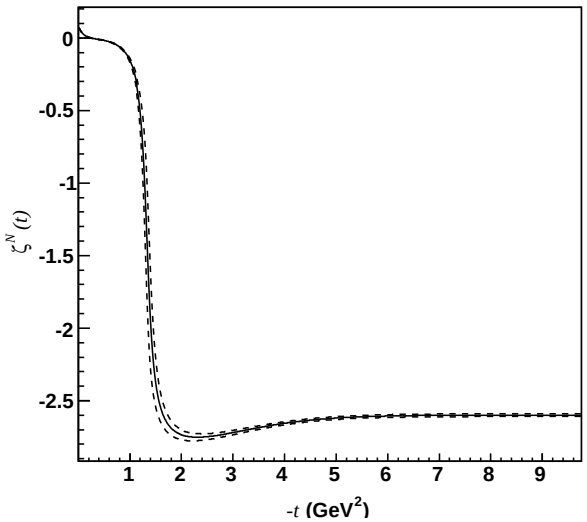

Figure 4.5: The hadronic phase $\zeta_B^N(s,t)$ corresponding to Fit B ($F_B^N(s,t)$, pp, $\sqrt{s} = 52.8$ GeV).

4.7 Comparison of the eikonal and WY formulas

To show the difference between the differential cross section $\frac{\mathrm{d}\sigma}{\mathrm{d}t}\big|_{eik}$ (see Eq. (4.6)) computed with use of more general formula (3.26) for complete elastic amplitude $F^{C+N}_{eik}(s,t)$ and the differential cross section $\frac{\mathrm{d}\sigma}{\mathrm{d}t}\big|_{WY} = \frac{\pi}{sp^2}\left|F^{C+N}_{WY}(s,t)\right|^2$ computed with use of the simplified WY formula (defined by Eqs. (3.16) and (3.17)) we will calculate the t-dependence of ratio

$$R(t) = \left| \frac{\frac{\mathrm{d}\sigma}{\mathrm{d}t}\big|_{eik} - \frac{\mathrm{d}\sigma}{\mathrm{d}t}\big|_{WY}}{\frac{\mathrm{d}\sigma}{\mathrm{d}t}\big|_{WY}} \right|. \tag{4.11}$$

To compute this quantity we need to know parameters σ_{tot}, ρ and B involved in the simplified WY formula. We will use the values of these parameters derived in [34] from experimental data, see Tab. 4.3. The ratio $R(t)$ is plotted in Fig. 4.6.

Data		pp	$\bar{p}p$
$\sqrt{s}$	[GeV]	52.8	541
σ_{tot}	[mb]	42.38 ± 0.15	62.2 ± 1.5
ρ		0.077 ± 0.009	0.135 ± 0.007
B	[GeV^{-2}]	12.87 ± 0.14	15.52 ± 0.07

Table 4.3: The values of the parameters involved in the simplified West-Yennie formula (3.17).

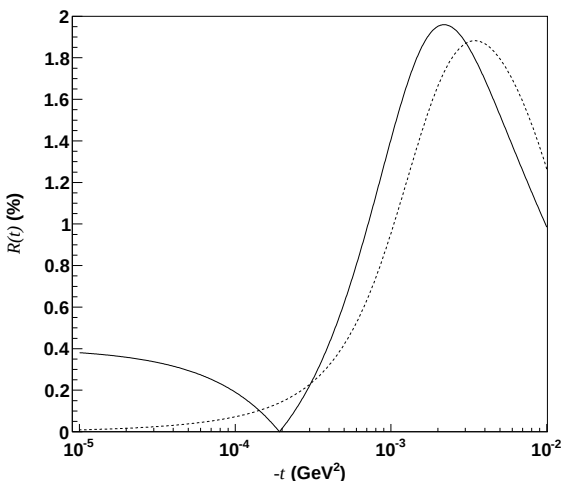

(a) solid line - Fit A_1; dashed line - Fit B

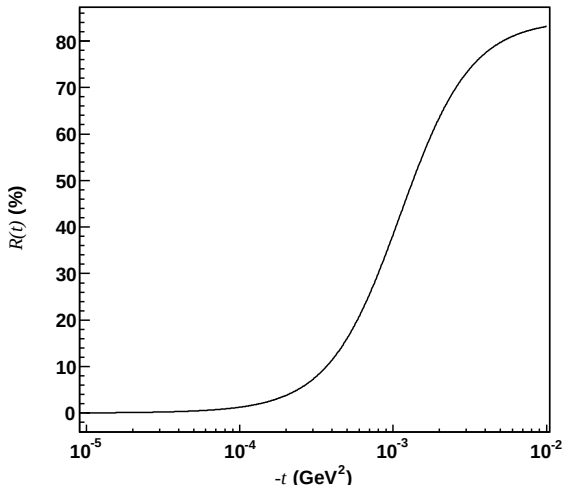

(b) Fit A_2

Figure 4.6: Ratio $R(t)$ defined by Eq. (4.11). (a) solid line corresponds to Fit A_1 ($F^N_A(s,t)$, pp, $\sqrt{s} = 52.8$ GeV) and dashed line corresponds to Fit B ($F^N_B(s,t)$, pp, $\sqrt{s} = 52.8$ GeV). (b) Fit A_2 ($F^N_A(s,t)$, $\bar{p}p$, $\sqrt{s} = 541$ GeV).

Our results plotted in Fig. 4.6 show that if an approach of the luminosity determination (see Chapter 3.5) is based on the estimation of simplified WY formula then the luminosity would be burdened by a non negligible systematic error. It was shown in [35] that the luminosity determination at the LHC (pp scattering at energy of $\sqrt{s} = 14$ TeV)

would be burdened by a systematic error approaching the value of $3.5 \div 4\%$ which overcomes the luminosity determination at the LHC planned to 1 - 1.5 %; see [1], [2] and [3].

4.8 Impact parameter space

It has been already mentioned that hadronic phase $\zeta^N(s,t)$ may influence the differential cross section $\frac{d\sigma}{dt}$ only weakly but it may have important consequences in the impact parameter space. It has been shown in [25] that the hadronic phase may lead to peripheral as well as central behavior of elastic collisions (see also Section 3.4). In the models analyzed in this thesis this impact parameter structure has been central where the distribution of elastic processes $|h_1(s,b)|^2$ has (for given s value) its maximum at impact parameter $b = 0$, i.e., for head-on collisions of two particles.

The elastic proton profile function $|h_1(s,b)|^2$ as well as function $g_1(s,b)$ (part of the inelastic overlap function $G_{inel}(s,b)$) and $\Im h_1(s,b)$ (part of the total distribution function), see Eq. (3.45) and (3.47), corresponding to Fit A_1, Fit A_2 and Fit B are shown in Fig. 4.7 and Fig. 4.8. The dashed lines again delimit the values of all the profiles within the statistical errors. We may see from the given graphs that both the models of hadronic amplitude $F_A^N(s,t)$ and $F_B^N(s,t)$ lead to the range of hadronic interaction around ≈ 2.5 fm.

As to the pp scattering at energy of 52.8 GeV the distribution function corresponding to hadron amplitude $F_A^N(s,t)$ with constant hadronic phase (Fit A_1) are very similar to the distribution functions corresponding to Brazil hadronic amplitude $F_B^N(s,t)$ with t-dependent hadronic phase (Fit B).

The correction function $K(s,b)$ given by Eq. (3.49) and corresponding to all three fits is plotted in Fig. 4.9. The function K is negligible in all cases in comparison to the corresponding function g_1.

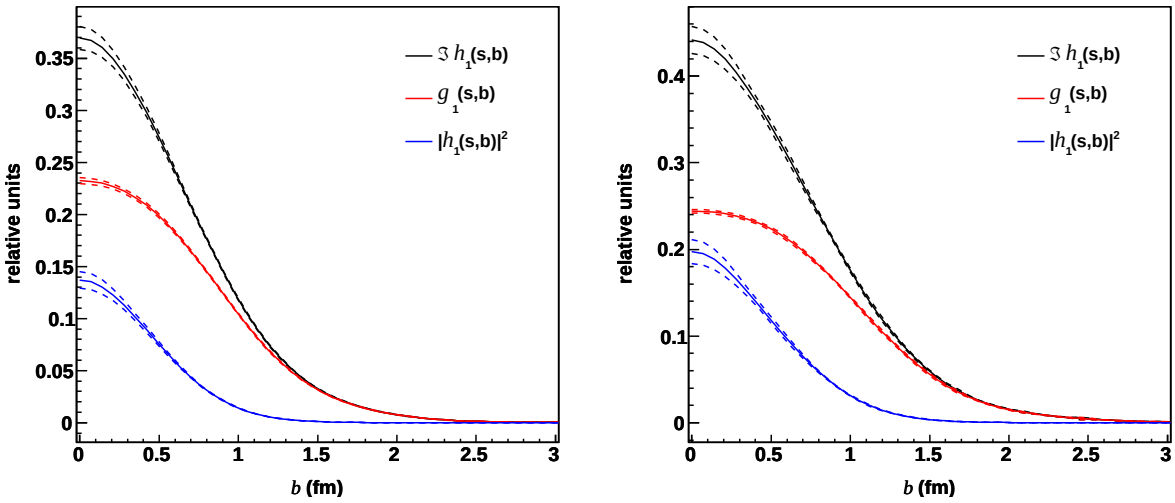

(a) Fit A_1 ($F_A^N(s,t)$, pp, $\sqrt{s} = 52.8$ GeV) (b) Fit A_2 ($F_A^N(s,t)$, $\bar{p}p$, $\sqrt{s} = 541$ GeV)

Figure 4.7: Impact parameter profile functions corresponding to Fit A_1 and Fit A_2, see Eqs. (3.45) and (3.47).

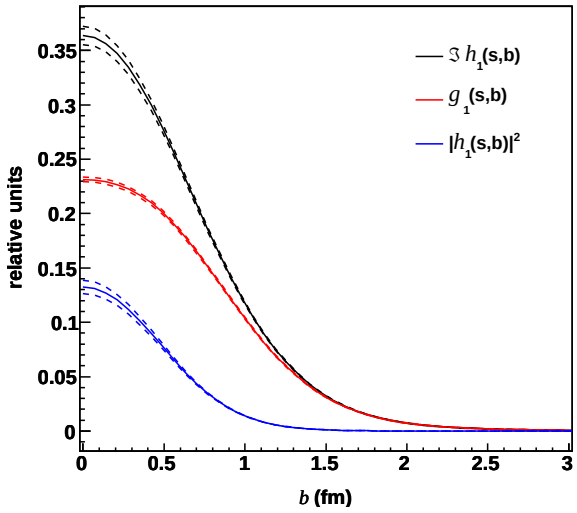

Figure 4.8: Impact parameter profile functions corresponding to Fit B ($F_B^N(s,t)$, pp, $\sqrt{s} = 52.8$ GeV), see Eqs. (3.45) and (3.47).

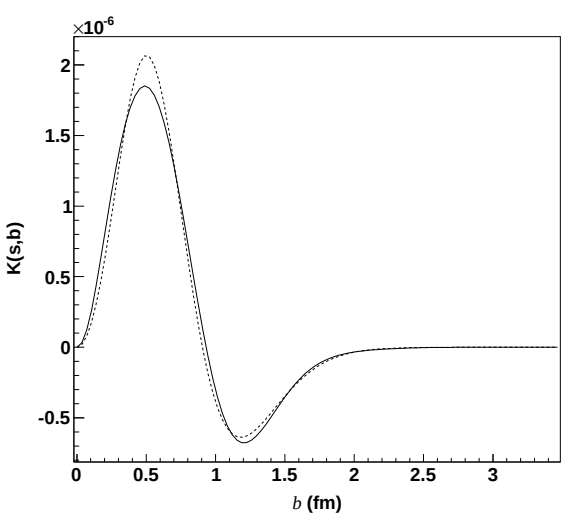

(a) solid line - Fit A_1; dashed line - Fit B

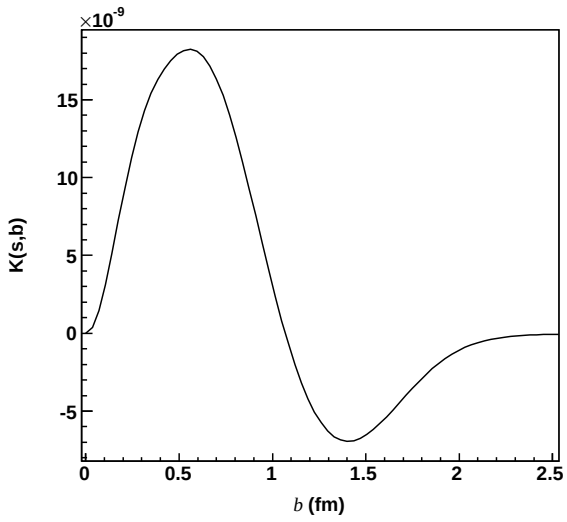

(b) Fit A_2 ($F_A^N(s,t)$, $\bar{p}p$, $\sqrt{s} = 541$ GeV)

Figure 4.9: Correction functions $K(s,b)$ defined by Eq. (3.49). (a) pp scattering, Fit A_1 (solid line) and Fit B (dashed line). (b) $\bar{p}p$ scattering, Fit A_2.

Values of the total, elastic and inelastic cross sections and root-mean-squares $\sqrt{\langle b^2(s)\rangle}$ determined on the basis of t-dependent hadronic amplitude $F_A^N(s,t)$ or $F_B^N(s,t)$ (see Chapter 3) and corresponding to all three fits are given in Tab. 4.4. Values of quantities $\rho(s,t=0)$ and $B(s,t=0)$ may be found also in Tab. 4.4.

The contributions of the phase $\langle b^2(s)\rangle_{ph}$ to $\langle b^2(s)\rangle_{el}$ (see Eq. (3.57)) corresponding to hadronic amplitude $F_A^N(s,t)$ are zero because this amplitude contains assumption of constant hadronic phase. In the case of Fit B with hadronic amplitude $F_B^N(s,t)$ the value of $\langle b^2(s)\rangle_{ph}$ is also quite negligible with respect to the contribution of the modulus $\langle b^2(s)\rangle_{mod}$. In both models the value of $\langle b^2(s)\rangle_{el}$ is determined practically only by the corresponding modulus of hadronic amplitude.

The values of root-mean-squares $\sqrt{\langle b^2(s)\rangle_{inel}}$ corresponding to all three fits are greater than $\sqrt{\langle b^2(s)\rangle_{el}}$; i.e., the elastic hadron scattering resulting from both models is more central than inelastic hadron scattering.

It follows from Eqs. (3.61) and (3.62) that some upper bounds exist for elastic and inelastic mean-squares. The inelastic upper bounds $\langle b^2(s)\rangle_{inel}^{bound}$ are practically saturated in both studied models, while values of elastic mean-squares $\langle b^2(s)\rangle_{el}$ lie significantly lower then corresponding values of $\langle b^2(s)\rangle_{el}^{bound}$. Similar result can by obtained also if the hadronic phase is parameterized according to Eq. (4.9) which also leads to central behavior of elastic hadron collisions, see [25].

		Fit A_1	Fit A_2	Fit B
Data		pp	$\bar{p}p$	pp
$F^N(s,t)$		$F_A^N(s,t)$	$F_A^N(s,t)$	$F_B^N(s,t)$
$\sqrt{s}$	[GeV]	52.8	541	52.8
$\rho(s,t=0)$		0.0648 ± 0.0054	0.11627 ± 0.00010	0.078
$B(s,t=0)$	[GeV^{-2}]	13.297 ± 0.045	16.4821 ± 0.0020	14.20 ± 0.13
σ_{tot}	[mb]	42.70 ± 0.21	62.71 ± 0.18	42.83 ± 0.21
σ_{inel}	[mb]	35.23 ± 0.16	49.53 ± 0.11	35.37 ± 0.15
σ_{el}	[mb]	7.46 ± 0.13	13.201 ± 0.087	7.460 ± 0.021
$\langle b^2(s)\rangle_{el}$	[fm^2]	0.4599 ± 0.0027	0.5712 ± 0.0086	0.4594 ± 0.0025
$\langle b^2(s)\rangle_{mod}$	[fm^2]	0.4599 ± 0.0027	0.5712 ± 0.0086	0.4580 ± 0.0025
$\langle b^2(s)\rangle_{ph}$	[fm^2]	0	0	0.001272 ± 0.000065
$\sqrt{\langle b^2(s)\rangle_{el}}$	[fm]	0.6782 ± 0.0020	0.7557 ± 0.0032	0.6778 ± 0.0018
$\sqrt{\langle b^2(s)\rangle_{tot}}$	[fm]	1.0176 ± 0.0017	1.1325 ± 0.0025	1.0560 ± 0.0049
$\sqrt{\langle b^2(s)\rangle_{inel}}$	[fm]	1.0758 ± 0.0017	1.2133 ± 0.0022	1.1196 ± 0.0053
$\langle b^2(s)\rangle_{inel}^{bound}$	[fm]	1.2549 ± 0.0047	1.6244 ± 0.0052	1.350 ± 0.012
$\langle b^2(s)\rangle_{el}^{bound}$	[fm]	5.923 ± 0.097	6.095 ± 0.061	6.404 ± 0.092

Table 4.4: Values of physically significant quantities corresponding to Fit A_1, Fit A_2 and Fit B.

Chapter 5

Conclusion

The presented thesis deals with two kinds of problems. The first one is contained in Chapter 2 and has been worked out during the stay of the author of this thesis at CERN. It is a part of studies concerning the response of the RP silicon detectors and representing one of the first steps towards developing a background suppression algorithm. The first insight into the proton background from the beam-beam interactions at $\beta^* = 0.5$ m has been obtained on the basis of detector response simulation. To see the response of the RP silicon detectors some statistics based on successfully reconstructed and fitted tracks for the most important particles from the simulation (protons, photons, neutrons, electrons, positrons and pions) have been presented.

The other part represents then some new results concerning two phenomenological models of elastic hadron amplitude and their consequences in the impact parameter space. The first model of hadron amplitude $F_A^N(s,t)$, which has been studied, contains the assumption of constant hadronic phase (i.e., constant quantity $\rho(s,t)$) in the whole region of kinematically allowed values of t. The second model of hadronic amplitude $F_B^N(s,t)$ (Brazil model) represents one of the present models with the hadronic phase that exhibits some stronger t-dependence. Both models have been fitted to experimental data represented by measured pp elastic differential cross section at energy of 52.8 GeV (Fit A_1 and Fit B). In the case of $F_A^N(s,t)$ additional fit at energy of 541 GeV ($\bar{p}p$ scattering) has been done (Fit A_2). To take both the Coulomb and hadron interaction into account in the whole region of kinematically allowed values of t, the eikonal formula (3.26) for the complete elastic amplitude $F_{eik}^{C+N}(s,t)$ has been used. The influence of the assumption of constant quantity $\rho(s,t)$ (involved in all approaches based on the simplified WY formula) have been thus tested also for greater values of t.

Althought the hadronic amplitudes $F_A^N(s,t)$ and $F_B^N(s,t)$ exhibit very different t-dependences of hadronic phase $\zeta^N(s,t)$ (one being constant and the second rather strongly t-dependent) they have similar effect on the description of elastic differential cross section. Choice of parameterization of modulus of hadronic amplitude $\left|F^N(s,t)\right|$ is thus much more significant in describing experimental data of differential cross section compared to parameterization of hadronic phase $\zeta^N(s,t)$.

It is commonly assumed that Coulomb scattering plays a role in a narrow region of small $|t|$ values only, while at all higher $|t|$ values it may be fully neglected. However, the interference ratios $f(s,t)$ corresponding to Fit A_2 and Fit B have an anomaly before and around the diffractive dip as we can see in Fig. 4.2. This effect shows that in the case of same models the Coulomb interaction may be non negligible also for higher values of $|t|$.

Our results plotted in Fig. 4.6 show then that also the luminosity can be burdened by a non negligible systematic error if an approach of the luminosity determination is based on the estimation of simplified WY formula.

The hadronic amplitudes $F_A^N(s,t)$ and $F_B^N(s,t)$ result in very similar behavior also in the impact parameter space. Both phenomenological models lead to central behavior of elastic collisions that may be hardly regarded as fully physical. The values of root-mean-squares $\sqrt{\langle b^2(s)\rangle_{inel}}$ corresponding to all three fits are greater than $\sqrt{\langle b^2(s)\rangle_{el}}$; i.e., the elastic hadron scattering resulting from the two models is more central than inelastic processes.

To perform all fits and more importantly to systematize different models and approaches describing elastic pp or $\bar{p}p$ scattering new program written in C++ has been developed. It may be used in fitting a hadronic amplitude $F^N(s,t)$ to measured pp or $\bar{p}p$ elastic differential cross section at given energy and for computing some other physically significant quantities. This new program re-implements many functions from FORTRAN programs developed in Ref. [5] in an object-oriented way and so its functionality may be easily extended.

Acronyms

CERN	European Organization for Nuclear Research
LHC	Large Hadron Collider being build at CERN
ISR	Intersecting Storage Rings
TOTEM	TOTal Elastic and diffractive cross section Measurement; one of the LHC experiments
CTS	Current Terminating Structure
RP	Roman Pot
IP5	Interaction Point 5
RP147	RP station at distances of +147 m from the IP5
RP220	RP station at distances of +220 m from the IP5
LSS	Long Straight Section
CASTOR	CERN Advanced STORage manager

References

[1] The TOTEM collaboration, Letter of Intent, CERN/LHCC 97-49, LHCC/I 11 (1997).

[2] The TOTEM collaboration, Technical Proposal, CERN/LHCC 99-7, LHCC/P5 (1999).

[3] The TOTEM collaboration, Technical Design Report, CERN-LHCC-2004-002 (2004).

[4] J. Kašpar, M. Deile, V. Avati, H. Niewiadomski and other people from TOTEM team, private communication.

[5] V. Kundrát and M. Lokajíček, Z. Phys. C 63 (1994) 619.

[6] J. Kašpar, High-energy diffraction processes - totem experiment, Master's thesis, Charles University, Prague, 2005.

[7] The TOTEM Collaboration, "The TOTEM Experiment at the LHC", 2008 JINST 3 S08007, doi: 10.1088/1748-0221/3/08/S08007 .

[8] The CMS and TOTEM diffractive and forward physics group, CERN-LHCC-2006-039.

[9] L. Evans and P. Bryant (editors), "LHC machine", 2008 jinst 3 s08001, doi: 10.1088/1748-0221/3/08/s08001.

[10] ROOT — An Object-Oriented Data Analysis Framework, http://root.cern.ch.

[11] H. Niewiadomski, Reconstruction of Protons in the TOTEM Roman Pot Detectors at the LHC, PhD thesis, Univ. Manchester, 2008.

[12] V. Barone and E. Predazzi, High-Energy Particle Diffraction (Springer, 2002).

[13] H. Pilkuhn, The Interaction of Hadron (North-Holldand, 1967).

[14] H. A. Bethe, Ann. Phys. 3 (1958) 190.

[15] G. B. West and D. R. Yennie, Phys. Rev. 172 (1968) 1413.

[16] M. P. Locher, Nucl. Phys. B2 (1967) 525.

[17] V. Kundrát, Elastic hadron scattering at high energies, Doctor of Mathematical and Physical sciences Thesis, Institute of Physics AV ČR, 1996.

[18] V. Kundrát and M. Lokajíček, Mod. Phys. Lett. A 11 (1996) 2241.

[19] V. Kundrát and M. Lokajíček, Phys. Lett. B 611 (2005) 102.

[20] V. Kundrát, M. Lokajíček and I. Vrkoč, Physics Letters B 656 (2007) 182 .

[21] R. J. Glauber, in Lectures in theoretical physics Vol.1 (Interscience Publishers N.Y, 1959).

[22] M.M. Islam In: A.O. Barut and W.E. Brittin (Eds.), Lectures in Theoretical Physics vol. 10B, Gordon and Breach (1968), p. 97.

[23] M. M. Islam, Nuclear Physics B 104 (1976) 511.

[24] F. Borkowski et al., Nucl. Phys. B 93 (1975) 461.

[25] V. Kundrát, M. Lokajíček and D. Krupa, Physics Letters B 544 (2002) 132.

[26] L. van Hove, Rev. Mod. Phys. 36 (1964) 655.

[27] P. A. S. Carvalho, A. F. Martini and M. J. Menon, European Physical Journal C 39 (2005) 359.

[28] R. F. Ávila and M. J. Menon, European Physical Journal C 54 (2008) 555, 0712.3398.

[29] J. Bystricky et al., in Nucleon-nucleon and kaon-nucleon scattering edited by H. Schopper (Landolt-Börnstein Series, Vol. 1), (Springer, Berlin, 1980).

[30] M. K. Carter, P. D. B. Collins and M. R. Whalley, Compilation of Nucleon-Nucleon and Nucleon-Antinucleon Elastic Scattering Data , RAL-86-002, preprint.

[31] UA4 data, D. Bernard et al.: Phys. Lett. 198B (1987) 583;
M. Bozzo et al.: Phys. Lett. 147B (1984) 385; 155B (1985) 197 .

[32] Minuit2 — Minimization Package,
http://seal.web.cern.ch/seal/MathLibs/Minuit2/html/ .

[33] F. James and M. Roos, Comput. Phys. Commun. 10 (1975) 343.

[34] N. Amos et al., Nucl. Phys. B 262 (1985) 689.

[35] V. Kundrát, J. Kašpar and M. Lokajíček, To the theory of high-energy nucleon collisions, Procceding of the Blois'O7/EDS07 Workshop on elastic and diffractiove Scattering, Hamburg, Germany (2007) p. 273.